

Strange processes in general two Higgs doublet model

Wei-Shu Hou and Girish Kumar

Department of Physics, National Taiwan University, Taipei 10617, Taiwan

E-mail: wshou@phys.ntu.edu.tw, girishk@hep1.phys.ntu.edu.tw

ABSTRACT: In the general two Higgs doublet model (g2HDM) that has extra Yukawa couplings, we analyze their New Physics (NP) contributions to kaon mixing parameter ε_K , direct CP violation parameter ε'/ε , and rare $K^+ \rightarrow \pi^+ \nu \bar{\nu}$, $K_L \rightarrow \pi^0 \nu \bar{\nu}$, and $K_{L,S} \rightarrow \mu^+ \mu^-$ decays. We study correlations between these observables, and call special attention to a unique complementarity of kaon mixing and rare $K \rightarrow \pi \nu \bar{\nu}$ decays in probing the exotic Higgs mass spectrum of g2HDM. The importance of kaon physics in probing NP vis-à-vis B physics is stressed. One unexpected feature we uncover is the special sensitivity of $K^+ \rightarrow \pi^+ \nu \bar{\nu}$ to TeV scale charged Higgs boson.

KEYWORDS: Kaons, Multi-Higgs Models, CP violation, Rare Decays

ARXIV EPRINT: [2207.07030](https://arxiv.org/abs/2207.07030)

Contents

1	Introduction	1
2	Relevant Interactions in the Model	3
3	Kaon Observables in g2HDM	4
3.1	Neutral kaon mixing	4
3.2	Kaon direct CPV	6
3.3	$K^+ \rightarrow \pi^+ \nu \bar{\nu}$ and $K_L \rightarrow \pi^0 \nu \bar{\nu}$	8
3.4	$K_{L,S} \rightarrow \mu^+ \mu^-$	10
4	Results	11
4.1	Effect of B sector and kaon CPV constraints	11
4.2	The normalized ratios $\mathcal{R}_\nu^{+,0}, \mathcal{R}_\mu^{L,S}$	13
4.3	$K \rightarrow \pi \nu \nu$ sensitivity to heavy charged Higgs	14
4.4	Correlations in $K \rightarrow \pi \nu \nu$ decays, and with $B_s \rightarrow \mu \mu$	16
5	Discussion and Summary	19
A	Loop Functions	20
B	Neutral B Meson Mixings and Mixing-induced CPV	21

1 Introduction

The general two Higgs doublet model (g2HDM) is one of the simplest NP models where one augments the Standard Model (SM) with another scalar SU(2) doublet [1] (see Ref. [2] for a review of 2HDMs). In contrast to the typical Type II 2HDM, which adopts an *ad hoc* Z_2 symmetry on Yukawa interactions to enforce the natural flavor conservation condition [3], no such discrete symmetry is imposed in g2HDM [4]. Consequently, in g2HDM there exists *extra* Yukawa couplings which are generic in size and complex in nature, with flavor-changing neutral Higgs (FCNH) couplings controlled by fermion mass-mixing hierarchies that are built-in by *Nature* herself. Of particular interest are extra Yukawa couplings related to the top quark, ρ_{tt} and ρ_{tc} , where they can provide new sources for charge-parity violation (CPV), which together with $\mathcal{O}(1)$ Higgs quartic couplings [5], can satisfy the Sakharov conditions [6] and give rise to electroweak baryogenesis (EWBG), i.e. account for the baryon asymmetry of the Universe (BAU), as illustrated in Refs. [7, 8].

An appealing aspect of EWBG in g2HDM is its testability at ongoing and upcoming collider and flavor experiments. For example, the couplings ρ_{tt} and ρ_{tc} at $\mathcal{O}(\lambda_t)$ strength with $\lambda_t \cong 1$ the SM top quark Yukawa coupling, can propel exquisite collider signatures

such as [9] $cg \rightarrow tH/tA \rightarrow tt\bar{c}$ (same-sign top plus c-jet) and $tt\bar{t}$ (triple-top), where H/A are CP-even/odd exotic neutral scalar bosons in g2HDM. Another important probe is charged Higgs (H^+) associated production: $cg \rightarrow bH^+ \rightarrow bt\bar{b}$ [10]. Besides ρ_{tc} and ρ_{tt} at $\mathcal{O}(1)$, this process is further enhanced at the amplitude level — in contrast to Type II 2HDM — by a CKM ratio $V_{tb}/V_{cb} \sim 24$, making it a unique probe of g2HDM. A review on prospects at LHC and the High-Luminosity LHC (HL-LHC) can be found in Ref. [11].

Another most promising probe of ρ_{tt} in the context of EWBG is the electric dipole moment (EDM) of the electron. An upper limit of $|d_e| < 1.1 \times 10^{-29} e \text{ cm}$ is set [12, 13] by ACME, which is the best limit on any EDM. The coupling ρ_{tt} contributes to electron EDM via two-loop (Barr-Zee) diagrams [14]. A hierarchy — similar to the one present in the SM — between g2HDM couplings of top and electron $|\rho_{ee}/\rho_{tt}| \propto \lambda_e/\lambda_t$ helps one evade [8] the ACME bound. Such direct correlations link EWBG realized at the very early Universe, to electron EDM being measured currently in the laboratories.

Similarly, quark flavor observables provide important probes of ρ_{ij} couplings. In the literature, B physics observables in particular have been discussed frequently to constrain g2HDM couplings. For example, precise measurements of neutral B_q ($q = s, d$) mixings [15] put stringent constraints on ρ_{ij} [16]; in particular, the off-diagonal down-type couplings get severely constrained [17]. The inclusive radiative decay $B \rightarrow X_s \gamma$ is known to be one of the most sensitive probes of H^+ . The measured value of its branching ratio $\mathcal{B}(B \rightarrow X_s \gamma) = (3.32 \pm 0.15) \times 10^{-4}$ [15] agrees well with its SM prediction [18]. For Type II 2HDM, the decay already sets the limit $m_{H^+} > 580 \text{ GeV}$ at 95% C.L. [19]. In contrast, $b \rightarrow s \gamma$ easily accommodates lower values of H^+ in g2HDM, but seriously constrains the parameter space for ρ_{ct} and the down coupling ρ_{bb} [16, 20].

Another often discussed process in the literature is the rare $B_s \rightarrow \mu^+ \mu^-$ decay. It is helicity-suppressed in the SM and therefore provides one of the most sensitive probes of scalar interactions. LHCb reported $\mathcal{B}(B_s \rightarrow \mu^+ \mu^-) = (3.09^{+0.46+0.15}_{-0.43-0.11}) \times 10^{-9}$ [21, 22], based on full dataset collected during Run 1 and Run 2 with integrated luminosity of 9 fb^{-1} in total. On the other hand, CMS has just reported their full Run 2 analysis based on 2016-2018 data, corresponding to an integrated luminosity of 140 fb^{-1} , giving $\mathcal{B}(B_s \rightarrow \mu^+ \mu^-) = (3.83^{+0.38+0.19+0.14}_{-0.36-0.16-0.13}) \times 10^{-9}$ [23], with central value about 1.2σ higher than LHCb result. These measurements agree with SM expectation [24, 25] and would put strong constraints on up-type ρ_{ij} couplings [26–28]. A previous combined analysis of ATLAS [29], CMS [30] and LHCb [31] based on 2011-2016 data found $\mathcal{B}(B_s \rightarrow \mu^+ \mu^-)_{\text{ave}} = (2.69^{+0.37}_{-0.35}) \times 10^{-9}$ [32], which is on the lower side of SM value, but now the trend has changed. In our numerical analysis, we will take the LHCb result as reference value, but also discuss briefly the implication of the CMS update.

Interestingly enough, $b \rightarrow s \ell^+ \ell^-$ data also exhibit significant tensions with SM in related $B \rightarrow K \ell \ell$, $K^* \ell \ell$ observables. Similarly, data related to charged current $b \rightarrow c \ell \nu$ also show deviations from SM. We refer to Ref. [33] for a recent summary about the *B anomalies* (see Ref. [34] for an experimental critique). The g2HDM is capable of addressing several of these B anomalies, where again the top couplings ρ_{tt} , ρ_{tc} , and ρ_{ct} play important roles. The $b \rightarrow s \ell \ell$ processes have been discussed in Refs. [27, 35, 36] while $b \rightarrow c \ell \nu$ are discussed in Refs. [26, 37, 38]. We caution that none of the deviations are confirmed

individually. Future data may yet decide the fate of the B anomalies.

Despite the intense scrutiny of g2HDM interactions as briefly outlined above, data still allows for sizable top-related ρ_{ij} [11]. We note, however, that a more robust probe of flavor structure of any NP model is through investigating correlations between NP contributions of different flavor sectors. This is particularly salient in case of g2HDM, where top-related ρ_{ij} couplings that contribute to flavor changing neutral coupling (FCNC) B processes would also affect other flavor sectors, most notably the kaon sector, which offers several observables that are very sensitive to NP contributions. We therefore analyze g2HDM contributions to various kaon processes and investigate the prospects.

The study of kaon physics has been instrumental historically in shaping our current understanding of SM (see Ref. [39, 40] for a review of kaon physics in SM). The ε_K parameter of neutral kaon mixing is very precisely measured, and along with mass differences ΔM_{B_q} ($q = s, d$) are among the most sensitive flavor probes of NP. The direct CPV parameter ε'/ε from $K \rightarrow \pi\pi$ decay is also a very sensitive probe of CP violating NP [41]. Back in 2015, RBC and UKQCD presented [42] their first lattice QCD result for $K \rightarrow \pi\pi$ matrix elements and found ε'/ε to be 2–3 σ below the experimental world average [43–45]. This result received much attention and prompted several NP analyses, such as in g2HDM [46–48]. However, the 2020 RBC-UKQCD [49] update of A_0 (isospin $I = 0$) matrix element for $K \rightarrow \pi\pi$ gave ε'/ε that is consistent with experiment. The theory uncertainties are still quite large, and significant NP contributions at $\lesssim \mathcal{O}(10^{-3})$ may still be accommodated [50].

On the other hand, rare $K^+ \rightarrow \pi^+\nu\bar{\nu}$ and $K_L \rightarrow \pi^0\nu\bar{\nu}$ decays are theoretically *clean* processes, with branching ratios very precisely determined in SM. Dominated by Z penguin and box diagrams in SM, they are highly suppressed, making them very sensitive probes of NP scale — even for scales beyond LHC reach. In contrast, rare decays $K_{L,S} \rightarrow \mu^+\mu^-$ have been less enthusiastically pursued in the literature, as they receive both short-distance (SD) and long-distance (LD) contributions; the LD contributions are dominated by two on-shell photons [51–54] and are quite significant. However, there has been important theoretical progress [53, 55] recently towards a reliable extraction of SD parameters using data, making these processes, in particular $K_S \rightarrow \mu^+\mu^-$, good probes of NP.

This paper is organized as follows. In the next section we introduce the Yukawa interactions in g2HDM and discuss the NP parameters relevant for our study. In Sec. 3, we discuss each of the aforementioned kaon observables in the context of g2HDM. Then, in Sec. 4 we discuss constraints from B physics and present our results for kaon observables. We summarize our conclusions in Sec. 5.

2 Relevant Interactions in the Model

As mentioned in the Introduction, g2HDM does not possess any discrete symmetry. Thus, the scalar doublets Φ_1 and Φ_2 are indistinguishable, and both couple to up-type as well as down-type SM fermions. Here, for convenience, we choose to work in the so-called Higgs basis, in which only one doublet receives vacuum expectation value (vev): $\langle\Phi_1\rangle \neq 0$, $\langle\Phi_2\rangle = 0$. After spontaneous symmetry breaking, the receiver of vev is identified with the SM Higgs doublet and participates in generating particle masses. The other doublet gives

rise to new interactions with fermions and interactions between the two Higgs doublets. In the physical basis, the Yukawa Lagrangian of the model is given as [56, 57],

$$\mathcal{L} = -\frac{1}{\sqrt{2}} \sum_{f=u,d,\ell} \bar{f}_i \left[(\lambda_i^f \delta_{ij} s_\gamma + \rho_{ij}^f c_\gamma) h + (\lambda_i^f \delta_{ij} c_\gamma - \rho_{ij}^f s_\gamma) H - i \operatorname{sgn}(Q_f) \rho_{ij}^f A \right] R f_j - \bar{u}_i \left[(V \rho^d)_{ij} R - (\rho^{u\dagger} V)_{ij} L \right] d_j H^+ - \bar{\nu}_i \rho_{ij}^\ell R \ell_j H^+ + h.c., \quad (2.1)$$

where we identify $h(125)$ with the discovered scalar at LHC, and H , A and H^\pm are exotic scalars which we assume to be heavier than h . The couplings $\lambda_i = \sqrt{2} m_i / v$ denote the SM Yukawa coupling, with m_i the fermion mass and $v = 246$ GeV the vev; ρ_{ij} are generic NP couplings, introduced already as extra Yukawa couplings; R , $L = (1 \pm \gamma_5)/2$ are chiral projections, and V is the Cabibbo-Kobayashi-Maskawa (CKM) matrix. The angle $c_\gamma \equiv \cos \gamma$ ($s_\gamma \equiv \sin \gamma$) describes the mixing between h and H . The limit $c_\gamma \rightarrow 0$, the so-called *alignment limit*, provides an additional mechanism [57] for suppressing FCNC involving the h boson, which implies that the discovered h boson approaches the SM Higgs boson.

As stated already, ρ_{ij} are generic in size and contain complex phases. However, the current data puts significant constraints on their strength. For example, neutral meson mixing data severely constrains off-diagonal entries of down type ρ_{ij}^d couplings [17], indicating that ρ^d matrix is almost diagonal in *Nature*. Further, data from proton-proton colliders such as the LHC already hint that u and d -quark related couplings have to be small. Interestingly, and as stressed already, the top-related couplings of g2HDM can be significantly larger [11]. On the other hand, lepton related ρ_{ij} are less constrained. But given the assumption that $\rho_{tt} \sim \mathcal{O}(\lambda_t)$ and $c_\gamma \sim \mathcal{O}(0.1)$, data from flavor violating processes such as $h \rightarrow \tau\mu$, $\tau \rightarrow \mu\gamma$, $\mu \rightarrow e\gamma$ and $\mu \rightarrow e$ conversion in nuclei suggest [28] $\rho_{\tau\tau}, \rho_{\tau\mu} \lesssim \mathcal{O}(\lambda_\tau)$ and $\rho_{e\ell} \lesssim \mathcal{O}(\lambda_e)$ ($\ell = e, \mu, \tau$), which are indeed very small.

We will therefore focus on the NP effects of only top- and charm-related couplings ρ_{tt} , ρ_{tc} , and ρ_{ct} , which mediate FCNC involving kaon at one loop. A more detailed discussion of experimental constraints on these couplings is postponed to Sec. 4.

3 Kaon Observables in g2HDM

3.1 Neutral kaon mixing

The original measure of CPV in $K \rightarrow \pi\pi$, the ε_K parameter, is rooted in the complex phase of neutral kaon mixing. Defining¹ $M_{12}^* = \langle \bar{K}^0 | \mathcal{H}_{\text{eff}}(\Delta S = 2) | K^0 \rangle$, one has

$$\varepsilon_K = \frac{\tilde{\kappa}_\epsilon e^{i\varphi_\epsilon}}{\sqrt{2}(\Delta M_K)_{\text{exp}}} (\operatorname{Im} M_{12}^{\text{SM}} + \operatorname{Im} M_{12}^{\text{NP}}) = e^{i\varphi_\epsilon} (\varepsilon_K^{\text{SM}} + \varepsilon_K^{\text{NP}}), \quad (3.1)$$

where the phase $\varphi_\epsilon = (43.51 \pm 0.05)^\circ$ [58], and correction factor $\tilde{\kappa}_\epsilon = 0.94 \pm 0.02$ [59] accounts for long distance effects. Note that $\varepsilon_K^{\text{SM}, \text{NP}}$ are real quantities.

¹A different normalization for external states so that $2m_K M_{12}^* = \langle \bar{K}^0 | \mathcal{H}_{\text{eff}}(\Delta S = 2) | K^0 \rangle$ is also widely used in the literature (see, for example, Ref. [39]).

Experimentally, ε_K has been determined with great accuracy [58],

$$|\varepsilon_K| = (2.228 \pm 0.011) \times 10^{-3}. \quad (3.2)$$

On the other hand, its prediction in SM is very sensitive to $|V_{cb}|$ (the leading SD effect is proportional to its 4th power) and therefore the precise determination depends on V_{cb} extracted from inclusive or exclusive $b \rightarrow c l \nu$ decays. Detailed analyses of $\varepsilon_K^{\text{SM}}$ can be found in Refs. [60–62]. The recent update in Ref. [62] finds $\varepsilon_K^{\text{SM}} = (2.16 \pm 0.18) \times 10^{-3}$. We impose the following [63] constraint on NP contributions to ε_K ,

$$\varepsilon_K^{\text{NP}} \equiv \kappa \times 10^{-3}, \quad \text{where } -0.2 \leq \kappa \leq 0.2, \quad (3.3)$$

On the other hand, ΔM_K is determined from the matrix element M_{12} as,

$$\Delta M_K = 2\text{Re } M_{12} \equiv 2[\text{Re } M_{12}^{\text{SM}} + \text{Re } M_{12}^{\text{NP}}]. \quad (3.4)$$

While $(\Delta M_K)_{\text{exp}} = (5.293 \pm 0.009) \times 10^{-3}$ [58] is precisely measured, the SM effect is dominated by the real part of the box diagrams involving charm quark and W exchange. The determination of ΔM_K^{SM} suffers significant uncertainties from QCD corrections to the SD part, and from the poorly known LD part [41], so we assign a 40% uncertainty.

In g2HDM, the NP contribution to kaon mixing arise from diagrams in Fig. 1, which generate the effective interaction [17],

$$\mathcal{H}_{\text{eff}} = [C_{HH} + C_{WH}](\bar{d}\gamma^\mu Ls)(\bar{d}\gamma^\mu Ls) + \text{h.c.}, \quad (3.5)$$

where C_{HH} is generated by H^+-H^- box diagrams,

$$C_{HH} = -\frac{(V_{k1}^* \rho_{kj} \rho_{lj}^* V_{l2})(V_{m1}^* \rho_{mi} \rho_{ni}^* V_{n2})}{128\pi^2 m_{H^+}^2} F_1(m_j^2/m_{H^+}^2, m_i^2/m_{H^+}^2), \quad (3.6)$$

and C_{WH} is generated by W^+-H^- box diagrams,

$$C_{WH} = \frac{g^2 m_j m_k (V_{j1}^* \rho_{ij}^* V_{i2})(V_{l1}^* \rho_{lk} V_{k2})}{128\pi^2 m_W^2 m_{H^+}^2} F_2(m_W^2/m_{H^+}^2, m_k^2/m_{H^+}^2, m_j^2/m_{H^+}^2), \quad (3.7)$$

where g is the weak coupling, and $F_1(x, y)$, $F_2(x, y, z)$ are given in Appendix A.

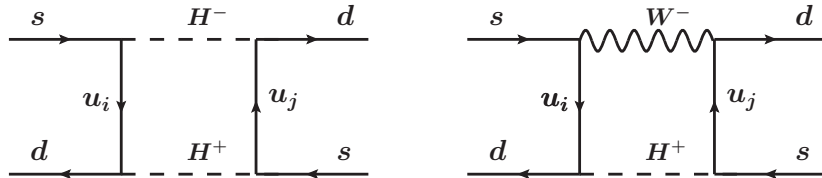


Figure 1. Sample $|\Delta S| = 2$ transitions induced by H^- in g2HDM.

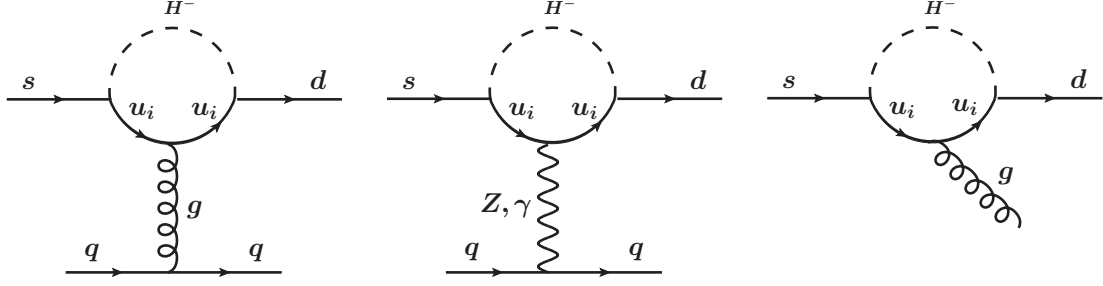


Figure 2. H^\pm induced contributions to ε'/ε in g2HDM. Another variant of the second diagram where Z, γ propagators couple to H^- is not shown.

3.2 Kaon direct CPV

The ε'/ε parameter is one of the important kaon observables which probes direct CPV in $K \rightarrow \pi\pi$ decays. It is convenient to discuss $K \rightarrow \pi\pi$ decays in terms of the isospin amplitudes $A_i = \langle (2\pi)_i | \mathcal{H}_{eff}(\mu) | K \rangle$ with $i = 1, 2$, and $\mu \sim 1$ GeV describes the physical scale. Then the formula for ε'/ε can be written as [64, 65],²

$$\text{Re} \left(\frac{\varepsilon'}{\varepsilon} \right) = -\frac{\omega_+}{\sqrt{2}|\varepsilon_K|} \left[\frac{\text{Im } A_0}{\text{Re } A_0} (1 - \Omega_{\text{eff}}) - \frac{\text{Im } A_2}{\text{Re } A_2} \right], \quad (3.8)$$

where $\omega_+ \equiv a (\text{Re } A_0 / \text{Re } A_2) = (4.53 \pm 0.02) \times 10^{-2} \simeq 1/22$, $a = 1.017$, and $\Omega_{\text{eff}} = (17.0 \pm 9.1) \times 10^{-2}$ [66] accounts for isospin breaking corrections. With lattice calculations of amplitudes A_2 [67] and A_0 [49] from RBC-UKQCD, one finds in SM,

$$(\varepsilon'/\varepsilon)_{\text{SM}} \times 10^4 = (21.7 \pm 2.6 \pm 6.2 \pm 5.0) = (21.7 \pm 8.4) \quad (\text{RBC-UKQCD 2020}), \quad (3.9)$$

where we add uncertainties in quadrature. On the other hand, chiral perturbation theory calculation gives [66],

$$(\varepsilon'/\varepsilon)_{\text{SM}} = (14 \pm 5) \times 10^{-4}, \quad (\chi\text{PT 2019}). \quad (3.10)$$

The current world average for ε'/ε from NA48 and KTeV gives [43–45],

$$(\varepsilon'/\varepsilon)_{\text{exp}} = (16.6 \pm 2.3) \times 10^{-4}, \quad (3.11)$$

which is consistent with the theoretical predictions in Eqs. (3.9) and (3.10).

The main contribution to ε'/ε in g2HDM comes from the first two diagrams in Fig. 2, which generate the following effective interactions,

$$\begin{aligned} -\mathcal{H}_{\text{eff}} = & \sum_{\substack{A=L,R \\ q=u,d}} C_{VLA}^q (\bar{d}\gamma^\mu Ls)(\bar{q}\gamma_\mu Aq) + \sum_{A=L,R} \tilde{C}_{VLA}^u (\bar{d}_\alpha \gamma^\mu Ls_\beta)(\bar{u}_\beta \gamma_\mu A u_\alpha) \\ & + C_{SLR}^d (\bar{d}Ls)(\bar{d}Rd) + \text{h.c.}, \end{aligned} \quad (3.12)$$

where we have suppressed color indices for color-singlet operators.

²For brevity of notation, we will use ε'/ε to denote $\text{Re}(\varepsilon'/\varepsilon)$.

The expressions of coefficients C_{VLA}^q related to $s \rightarrow du\bar{u}$ are as follows:

$$C_{VLL}^u = - \left[g_s^2 G_{\gamma 1}(z_i) - 4e^2 G_{\gamma 12}(z_i) + g^2(-3 + 4s_W^2) \frac{m_{H^+}^2}{m_W^2} G_Z(z_i) \right] \frac{V_{i1}^* \rho_{ij} \rho_{kj}^* V_{k2}}{96\pi^2 m_{H^+}^2}, \quad (3.13)$$

$$C_{VLR}^u = - \left[g_s^2 G_{\gamma 1}(z_i) - 4e^2 G_{\gamma 12}(z_i) + 4g^2 s_W^2 \frac{m_{H^+}^2}{m_W^2} G_Z(z_i) \right] \frac{V_{i1}^* \rho_{ij} \rho_{kj}^* V_{k2}}{96\pi^2 m_{H^+}^2}, \quad (3.14)$$

$$\tilde{C}_{VLL}^u = \tilde{C}_{VLR}^u = g_s^2 \frac{V_{i1}^* \rho_{ij} \rho_{kj}^* V_{k2}}{32\pi^2 m_{H^+}^2} G_{\gamma 1}(z_i), \quad (3.15)$$

while those related to $s \rightarrow d\bar{d}$ are given by,

$$C_{VLL}^d = - \left[-2g_s^2 G_{\gamma 1}(z_i) + 2e^2 G_{\gamma 12}(z_i) + g^2(3 - 2s_W^2) \frac{m_{H^+}^2}{m_W^2} G_Z(z_i) \right] \frac{V_{i1}^* \rho_{ij} \rho_{kj}^* V_{k2}}{96\pi^2 m_{H^+}^2}, \quad (3.16)$$

$$C_{VLR}^d = - \left[g_s^2 G_{\gamma 1}(z_i) + 2e^2 G_{\gamma 12}(z_i) - 2g^2 s_W^2 \frac{m_{H^+}^2}{m_W^2} G_Z(z_i) \right] \frac{V_{i1}^* \rho_{ij} \rho_{kj}^* V_{k2}}{96\pi^2 m_{H^+}^2}, \quad (3.17)$$

$$C_{SLR}^d = -2\tilde{C}_{VLR}^u. \quad (3.18)$$

Here g_s , e , g arise from g -, γ - and Z -penguin diagrams, respectively, and repeated indices are summed over. The loop functions $G_{\gamma 1, \gamma 12, Z}(x)$ are listed in Appendix A.

The last diagram in Fig. 2 give rise to the chromo-magnetic dipole interaction:

$$\mathcal{H}_{\text{eff}} = -C_{8g} m_s (\bar{d} \sigma_{\mu\nu} T^a R s) G_{\mu\nu}^a + \text{h.c.}, \quad (3.19)$$

where coefficient C_{8g} is

$$C_{8g} = g_s \frac{V_{i1}^* \rho_{ij} \rho_{kj}^* V_{k2}}{32\pi^2 m_{H^+}^2} F_{\sigma_1}(m_i^2/m_{H^+}^2), \quad (3.20)$$

where the loop function $F_{\sigma_1}(x)$ is given in Appendix A. But we note that the dipole operator contribution in our case is very small compared to those from Eq. (3.12) and can be ignored.

The NP contribution to $(\varepsilon'/\varepsilon)_{\text{NP}}$ can be calculated from the following formula [50]:³

$$(\varepsilon'/\varepsilon)_{\text{NP}} = \sum_i P_i(\mu_{\text{EW}}) \text{Im}[C_i^*(\mu_{\text{EW}}) - C_i'^*(\mu_{\text{EW}})] \times (1 \text{ TeV})^2, \quad (3.21)$$

where $\mu_{\text{EW}} \simeq 160 \text{ GeV}$ corresponds to the electroweak scale, and the P_i factors capture information of hadronic matrix elements $\langle(\pi\pi)_I|O_i K\rangle$. The numerical values of P_i , evaluated using matrix elements provided by RBC-UKQCD [49, 67], are given in Ref. [50]. Since the Wilson coefficients $C_i^{(\prime)}$ in Eq. (3.21) are defined at the electroweak scale, but those in Eqs. (3.12) and (3.19) are at NP scale μ_{NP} , one needs to evolve $C_i^{(\prime)}(\mu_{\text{NP}})$ down to the electroweak scale using renormalization group equations (RGE) before using the NP formula given in Eq. (3.21). Note also that though operators with $q = s, c, b$ in Eq. (3.12) do not arise at the $K \rightarrow \pi\pi$ factorization scale, they can contribute through RGE above

³Note that \mathcal{H}_{eff} in Ref. [50] has the form $\sum_i C_i/(1 \text{ TeV})^2 (\bar{s}\Gamma_i d)(\bar{q}\Gamma_i q)$, while we have $\sum_i C_i(\bar{d}\Gamma_i s)(\bar{q}\Gamma_i q)$. Therefore, Eq. (3.21) contains complex-conjugate Wilson coefficients rescaled by $(1 \text{ TeV})^2$ compared to the similar expression given in Ref. [50].

this scale [68]. But as their contribution turns out to be very small compared to the ones with $q = u, d$ [50], we ignore these operators for simplicity.

As already stated, the latest SM prediction for ε'/ε agrees well with the experimental value. But the uncertainties in both values, especially theory, are quite large at present, which allows the following range of values from NP contributions [50],

$$-4 \times 10^{-4} \lesssim (\varepsilon'/\varepsilon)_{\text{NP}} \lesssim 10 \times 10^{-4}. \quad (3.22)$$

3.3 $K^+ \rightarrow \pi^+ \nu \bar{\nu}$ and $K_L \rightarrow \pi^0 \nu \bar{\nu}$

The branching ratio of $K^+ \rightarrow \pi^+ \nu \bar{\nu}$ in the SM is given as [72],

$$\mathcal{B}(K^+ \rightarrow \pi^+ \nu \bar{\nu}) = \kappa_+ (1 + \delta_{\text{EM}}) \left\{ \left(\frac{\text{Im}[v_t X(x_t)]}{\lambda^5} \right)^2 + \left(\frac{\text{Re}[v_c]}{\lambda} P_c + \frac{\text{Re}[v_t X(x_t)]}{\lambda^5} \right)^2 \right\}. \quad (3.23)$$

Here $\lambda \equiv |V_{us}|$, $v_i \equiv V_{is}^* V_{id}$ are CKM factors, $\delta_{\text{EM}} = -0.003$ accounts for radiative corrections to the decay, and the factor $\kappa_+ = (5.173 \pm 0.025)(\lambda/0.025)^8 \times 10^{-11}$ [72] contains information about FCNC hadronic matrix elements obtained from semileptonic decays of kaons [73]. The loop function $X(x_t) = 1.462 \pm 0.017$ [74], where $x_t = m_t^2/m_W^2$, contains pure SD from top quark while $P_c = (0.405 \pm 0.024)(0.225/\lambda)^4$ [75–79] includes both SD and LD contributions from charm quark.

For the SM branching ratio of $K^+ \rightarrow \pi^+ \nu \bar{\nu}$, we obtain,

$$\mathcal{B}(K^+ \rightarrow \pi^+ \nu \bar{\nu})_{\text{SM}} = (9.07 \pm 0.82) \times 10^{-11}, \quad (3.24)$$

which is consistent with the commonly cited value of Ref. [72], whereas a more recent analysis [74] finds a lower but more precise value of $(7.7 \pm 0.6) \times 10^{-11}$ in SM. The uncertainties in SM are dominated by the CKM parameters V_{cb} and phase angle γ [72].

On the experimental side, NA62 has reported [80],

$$\mathcal{B}(K^+ \rightarrow \pi^+ \nu \bar{\nu})_{\text{exp}} = (10.6_{-3.4}^{+4.0} \pm 0.9) \times 10^{-11}, \quad (3.25)$$

where the first error is statistical and the second systematic. The measurement is based on data collected during the 2016-2018 runs and improves the previous measurement by E949 at Brookhaven [81]. Eq. (3.25) agrees within 1σ of Eq. (3.24), but the large statistical error still allows significant NP contribution. NA62 will continue collecting data in the next few years, and aims at measuring the branching ratio to 10% precision by 2024 [82].

In g2HDM, the Z -penguin diagrams with H^\pm in the loop as shown in Fig. 3, generate a purely left-handed effective interaction as in SM,

$$\mathcal{H}_{\text{eff}} = \frac{4 G_F}{\sqrt{2}} C_{LL}^{a,b} (\bar{s} \gamma_\mu L d) (\bar{\nu}_a \gamma^\mu L \nu_b) + \text{h.c.}, \quad (3.26)$$

where a, b denote neutrino flavors. The Wilson coefficient $C_{LL}^{a,b}$ is⁴

$$C_{LL}^{a,b} = -\frac{\delta_{ab}}{16\pi^2} (V^\dagger \rho_u)_{2i} (\rho_u^\dagger V)_{i1} G_Z(m_i^2/m_{H^\pm}^2). \quad (3.27)$$

⁴Our result for $C_{LL}^{a,b}$ in Eq. (3.27) differs from Ref. [48] by a factor of 2; checking with the authors, they agree with our formula. Our result agrees with the corresponding expression of Ref. [83], but these authors took the limit of diagonal ρ^u , which differs from our case.

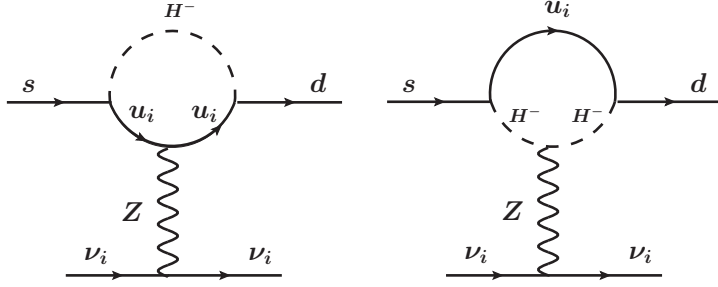


Figure 3. H^- induced Z -penguin contributions to $s \rightarrow d\nu\bar{\nu}$ in g2HDM.

where the loop function G_Z is given in Appendix A.

The g2HDM modification to SM branching ratio is effected by the simple replacement,

$$X(x_t) \rightarrow X_{\text{eff}} \equiv X(x_t) + \frac{2\pi s_W^2}{\alpha v_t} C_{LL}^{a,b}, \quad (3.28)$$

where s_W is the Weinberg angle and α the fine structure constant.

For the CP-violating decay $K_L \rightarrow \pi^0 \nu \bar{\nu}$, the SM result is [72],

$$\mathcal{B}(K_L \rightarrow \pi^0 \nu \bar{\nu}) = \kappa_L \left(\frac{\text{Im}[v_t X(x_t)]}{\lambda^5} \right)^2, \quad (3.29)$$

where $\kappa_L = (2.231 \pm 0.013)(\lambda/0.025)^8 \times 10^{-10}$, with remaining parameters defined already. Eq. (3.29) is completely dominated by SD top contribution with charm contribution negligible, leading to a more accurate prediction of branching ratio. Within SM, we obtain

$$\mathcal{B}(K_L \rightarrow \pi^0 \nu \bar{\nu})_{\text{SM}} = (3.24 \pm 0.36) \times 10^{-11}, \quad (3.30)$$

consistent with commonly cited result of Ref. [72], where theory uncertainties are again dominated by CKM parameters, with $|V_{ub}|$ contributing the most [72]. The analysis in Ref. [74] obtains a slightly lower central value $\mathcal{B}(K_L \rightarrow \pi^0 \nu \bar{\nu})_{\text{SM}} = (2.59 \pm 0.29) \times 10^{-11}$.

The KOTO experiment at J-PARC sets a 90% C.L. bound [84] of

$$\mathcal{B}(K_L \rightarrow \pi^0 \nu \bar{\nu})_{\text{exp}} < 4.9 \times 10^{-9}, \quad (3.31)$$

which is based on data collected during 2016-2018, where three candidate events were observed in the signal region. KOTO subsequently uncovered contamination from K^\pm and scattered K_L decays, giving a total number of 1.22 ± 0.26 background events [84]. Having identified the potential source of the three observed events, it led to a weaker bound than the single event sensitivity. A previous analysis based on a *smaller* data set collected in 2015 gave a slightly better bound of $\mathcal{B}(K_L \rightarrow \pi^0 \nu \bar{\nu})_{\text{exp}} < 3.0 \times 10^{-9}$ [85], in good part because no signal events were observed.

The future prospect for the measurement of $K_L \rightarrow \pi^0 \nu \bar{\nu}$ is rather good. KOTO will resume data collection and expects to measure the decay at SM sensitivity in the next few years [86]. A proposed experiment KLEVER [87] at CERN plans to measure the decay at

$\sim 20\%$ precision. There is also the proposal for KOTO Step-2 [88, 89], aiming at single event sensitive of $\mathcal{O}(10^{-13})$ to measure the decay rate.

The g2HDM modification of the SM branching ratio, Eq. (3.29), is achieved by replacing $X(x_t)$ according to Eq. (3.28), just as for $K^+ \rightarrow \pi^+ \nu \bar{\nu}$.

3.4 $K_{L,S} \rightarrow \mu^+ \mu^-$

With effective hamiltonian for $K^0 \rightarrow \mu^+ \mu^-$ defined as,

$$\mathcal{H}_{\text{eff}} = -C_A(\bar{s}\gamma^\mu P_L d)(\mu\gamma_\mu\gamma_5\mu) + \text{h.c.}, \quad (3.32)$$

the branching ratio for $K_L \rightarrow \mu^+ \mu^-$ is given by [70],

$$\mathcal{B}(K_L \rightarrow \mu^+ \mu^-) = \tau_L \frac{f_K^2 m_K m_\mu^2 \beta_\mu}{4\pi} \left| \text{Re}(C_A) - \frac{G_F^2 m_W^2}{\pi^2} A_{L\gamma\gamma}^\mu \right|^2, \quad (3.33)$$

where the first term corresponds to the SD contribution and the second represents LD contributions, with τ_L the K_L lifetime [58], f_K the decay constant [71], and $\beta_\mu = \sqrt{1 - 4m_\mu^2/m_K^2}$. Within SM, $C_A^{\text{SM}} = -(G_F^2 m_W^2/\pi^2)(v_t Y_t + v_c Y_c)$, where $Y_t = 0.950 \pm 0.049$ and $Y_c = (2.95 \pm 0.46) \times 10^{-4}$ denote contributions from top and charm quarks, respectively [69], while the LD contributions have been studied in Refs. [51–54].

The numerical value of $A_{L\gamma\gamma}^\mu$ can be found in Ref. [70], but the sign of $A_{L\gamma\gamma}^\mu$ is not known, which can be constructive (–) or destructive (+) with the SD contribution. The corresponding predictions in the SM are [51–53, 69],

$$\mathcal{B}(K_L \rightarrow \mu^+ \mu^-)_{\text{SM}} = \begin{cases} (8.11 \pm 0.49 \pm 0.13) \times 10^{-9}, & (\text{for } - \text{ sign}) \\ (6.85 \pm 0.80 \pm 0.06) \times 10^{-9}, & (\text{for } + \text{ sign}) \end{cases} \quad (3.34)$$

where the first uncertainty is from LD contribution, while the second contains parametric uncertainties from e.g. CKM elements. A precise measurement of $K_{L,S} \rightarrow \mu^+ \mu^-$ interference can help [53] determine the sign of $A_{L\gamma\gamma}^\mu$.

Based on Refs. [90–92], the world average for $\mathcal{B}(K_L \rightarrow \mu^+ \mu^-)$ is [58],

$$\mathcal{B}(K_L \rightarrow \mu^+ \mu^-)_{\text{exp}} = (6.84 \pm 0.11) \times 10^{-9} \quad (\text{PDG 2020}), \quad (3.35)$$

which is measured to 1.6% precision and seem to favor destructive interference from LD effect. The g2HDM contributions to $K_L \rightarrow \mu^+ \mu^-$ are dominated by the same diagrams as in Fig. 3, but with $Z\nu\nu$ vertex replaced by $Z\mu\mu$. The γ -penguin diagrams are absent due to a Ward identity for on-shell leptons. The corresponding contribution to C_A is,

$$C_A^{\text{NP}} = \frac{G_F}{8\sqrt{2}\pi^2} V_{i2}^* \rho_{ij} \rho_{kj}^* V_{k1} G_Z(x_i). \quad (3.36)$$

The $K^0 \rightarrow e^+ e^-$ decay is suppressed by m_e^2/m_μ^2 compared with dimuons.

The $K_S \rightarrow \mu^+ \mu^-$ rate depends on the imaginary part of SD contributions, hence a sensitive probe of NP with complex phases. The branching ratio is [53],

$$\mathcal{B}(K_S \rightarrow \mu^+ \mu^-) = \tau_S \frac{f_K^2 m_K m_\mu^2 \beta_\mu}{4\pi} \left[(\text{Im}(C_A))^2 + \left| \frac{\beta_\mu G_F^2 m_W^2}{\pi^2} B_{S\gamma\gamma}^\mu \right|^2 \right], \quad (3.37)$$

with C_A as defined in Eq. (3.32), and $B_{S\gamma\gamma}^\mu$ arises [53] from LD effects, which only add in quadrature to SD. The rate is suppressed by the K_S lifetime, τ_S , down to [51–53, 69],

$$\mathcal{B}(K_S \rightarrow \mu^+ \mu^-)_{\text{SM}} = (4.99_{\text{LD}} + 0.19_{\text{SD}}) \times 10^{-12} = (5.2 \pm 1.5) \times 10^{-12}. \quad (3.38)$$

The current upper limit by LHCb [93] at 90% C.L. is $\mathcal{B}(K_S \rightarrow \mu^+ \mu^-) < 2.1 \times 10^{-10}$, which improves their previous bound [94] by a factor of four. LHCb Upgrade II will improve the limit to below $\mathcal{O}(10^{-11})$, and should approach SM sensitivity [95].

4 Results

For our numerical study, relevant parameters are the complex extra Yukawa couplings ρ_{tt} , ρ_{tc} , ρ_{ct} , and the charged Higgs mass m_{H^+} . We use the software package `Flavio` [96]; all Wilson coefficients are adapted to *flavio basis* [97], then QCD-evolved from high scale to the relevant process scale using the package `Wilson` [98]. For extra Higgs boson masses in g2HDM, sub-TeV values are favored for strongly first order electroweak phase transitions in the early Universe [5, 7, 8]. But as we will see later, rare kaon decays offer excellent probes of *heavier* H^+ . Therefore, we give results for $m_{H^+} = 400$ and 1000 GeV, and refer to the former as light H^+ scenario, while the latter is called the heavy H^+ scenario.

4.1 Effect of B sector and kaon CPV constraints

We first consider constraints from B sector. We list the B meson observables considered and the corresponding measurements in Table 1. The g2HDM formulas for $B \rightarrow X_s \gamma$ and $B_s \rightarrow \mu^+ \mu^-$ decay branching ratios can be found in many works (see, for example, Refs. [26, 27, 36]). The discussion of neutral B_q ($q = s, d$) mass difference ΔM_{B_q} and mixing-induced CP asymmetries $S_{\psi K_S}$ and $S_{\psi\phi}$ as probes of B_q -mixing phases from $B_d \rightarrow \psi K_S$ and $B_s \rightarrow \psi\phi$, respectively, is relegated to Appendix B.

In Fig. 4, we illustrate 2σ constraints from B observables in the ρ_{ct} - ρ_{tt} plane, where the relatively weak bound from $S_{\psi\phi}$ is not shown. To contrast with B sector, we show also the region (red) allowed by ε_K using Eq. (3.3) (recall $\varepsilon_K^{\text{NP}} = \kappa \times 10^{-3}$). For light $m_{H^+} = 400$ GeV, the B sector rules out significant portions of parameter space, but still allows large values of ρ_{tt} and ρ_{ct} , especially along the axes, i.e. in regions where one of the couplings is vanishing. But as seen from Fig. 4, ε_K provides the most severe constraint.

Observable	Measurement
ΔM_{B_s}	$(17.741 \pm 0.020) \text{ ps}^{-1}$ [58]
ΔM_{B_d}	$(0.5065 \pm 0.0019) \text{ ps}^{-1}$ [58]
$S_{\psi K_S}$	(0.699 ± 0.017) [15]
$S_{\psi\phi}$	(0.050 ± 0.019) [15]
$\mathcal{B}(B \rightarrow X_s \gamma)$	$(3.32 \pm 0.15) \times 10^{-4}$ [15]
$\mathcal{B}(B_s \rightarrow \mu^+ \mu^-)$	$(3.09^{+0.46+0.15}_{-0.43-0.11}) \times 10^{-9}$ [22]

Table 1. Experimental data of various B meson observables.

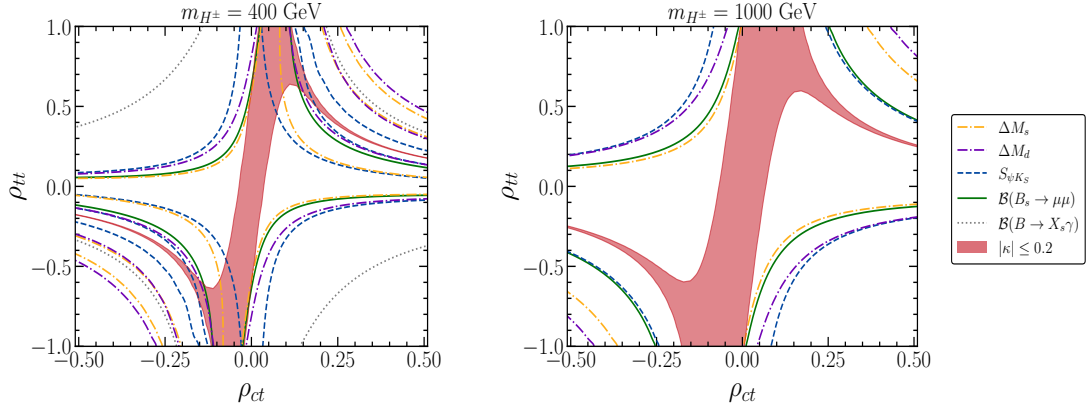


Figure 4. B sector and ε_K constraints in ρ_{ct} - ρ_{tt} plane for $m_{H^+} = 400$ and 1000 GeV. Colored lines indicate 2σ range of experimental data, outside of which are ruled out. The filled red band corresponds to the region allowed by $\varepsilon_K^{\text{NP}}$.

Combined with the B sector, it essentially rules out a sizable ρ_{ct} , but ρ_{tt} can still be quite large since ε_K has weaker sensitivity to ρ_{tt} compared with ρ_{ct} . However, for heavy $m_{H^+} = 1000$ GeV, the B sector bounds weaken while the region allowed by ε_K broadens. But now ε_K truly becomes the leading constraint in the whole parameter space. From Fig. 4, one also notes that contributions from ρ_{tt} and ρ_{ct} to ε_K (also to ΔM_{B_q} and $S_{\psi K_S}$) tend to cancel each other, as reflected in the narrow red bands for large ρ_{ct} in heavy H^+ case.

In Fig. 4, ρ_{ct} and ρ_{tt} are taken as real. But the essence of Yukawa couplings are their complexity. Allowing complex phases, the cancellation region hence allowed parameter space changes. To explore g2HDM effects in the kaon sector, we perform a parameter scan that takes the phases of $\phi_{ij} \equiv \arg \rho_{ij}$ into account. Specifically, we scan over:

$$|\rho_{tt}|, |\rho_{tc}| \in [0, 1], \quad \phi_{tt}, \phi_{tc} \in [-\pi, \pi]; \quad |\rho_{ct}| \in [0, 0.3], \quad \phi_{ct} \in [-\pi, \pi]. \quad (4.1)$$

Each parameter is varied uniformly to generate a sample size of a quarter million random points. The smaller range of $|\rho_{ct}|$ is chosen from hindsight, that combined flavor constraints on ρ_{ct} will rule out values larger than ~ 0.2 , as will be shown later. Fixing to narrower range also means we can obtain a denser population of allowed points.

In Fig. 5, we show the scatter plot obtained in the $\varepsilon_K^{\text{NP}}$ vs $(\varepsilon'/\varepsilon)_{\text{NP}}$ plane. We purposely show parameter ranges that are far larger than allowed by data to illustrate the complementarity of the kaon sector as sensitive probes of ρ_{ij} couplings. The blue (yellow) points are allowed (disallowed) by B physics data. For light H^+ (left), B sector basically rules out negative values of κ , but is less efficient in constraining positive κ values. For $(\varepsilon'/\varepsilon)_{\text{NP}}$, we notice an almost opposite situation: there is more population of scatter points corresponding to large and negative $(\varepsilon'/\varepsilon)_{\text{NP}}$ values, while relatively few points for positive $(\varepsilon'/\varepsilon)_{\text{NP}}$. For heavy H^+ case (right), the spread of the allowed points has shrunk because heavy H^+ suppresses NP contribution to κ and ε'/ε , but now negative κ values are also possible, because of relative inefficiency of B sector in constraining ρ_{ct} . We will expound on the significance of sizeable ρ_{ct} later when we discuss $s \rightarrow d\nu\nu$ processes.

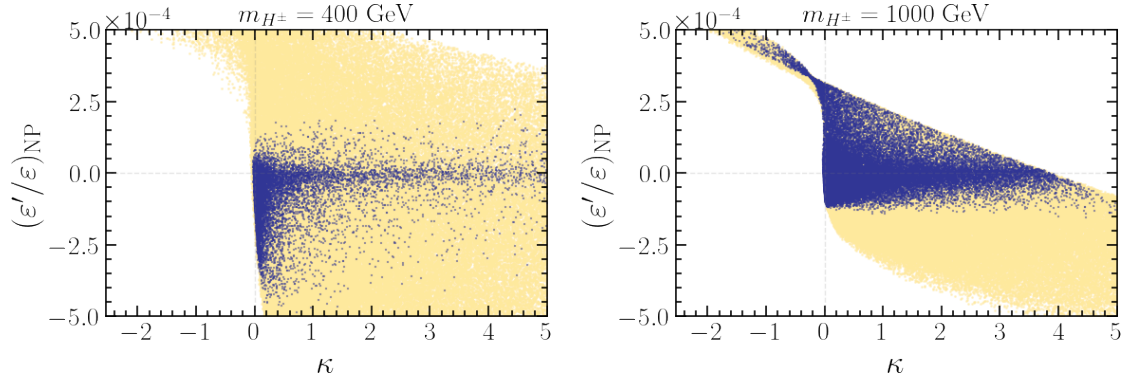


Figure 5. Scatter plot showing range of values accessible in g2HDM for $\varepsilon_K^{\text{NP}}$ and $(\varepsilon'/\varepsilon)_{\text{NP}}$ from parameter scan using Eq. (4.1). The yellow points are obtained with no experimental constraint imposed, while blue points are obtained after imposing B sector constraints of Table 1.

We note that constraints from B sector alone already restrict ε'/ε values to the range $-5 \times 10^{-4} \lesssim (\varepsilon'/\varepsilon)_{\text{NP}} \lesssim 2 \times 10^{-4}$ for light H^+ , and $-1 \times 10^{-4} \lesssim (\varepsilon'/\varepsilon)_{\text{NP}} \lesssim 5 \times 10^{-4}$ for heavy H^+ , consistent with current data (Eq. (3.22)). The maximum positive $(\varepsilon'/\varepsilon)_{\text{NP}}$ is $\sim 3 \times 10^{-4}$ in heavy H^+ case after one imposes the $|\kappa| < 0.2$ constraint from ε_K data (Eq. (3.3)). On the other hand, for light H^+ case, we note that although positive $(\varepsilon'/\varepsilon)_{\text{NP}}$ of order $\mathcal{O}(10^{-4})$ can be reached, larger negative contributions are far more preferred, regardless of ε_K constraint. Figs. 4 and 5 underline the point that ε_K provides complementary — much better in many cases — constraints on ρ_{ij} , and therefore must be included in any phenomenological study of g2HDM. In the following parameter scans, we impose the $\varepsilon_K^{\text{NP}}$ constraint from Eqs. (3.3) along with B physics constraints of Table 1.

4.2 The normalized ratios $\mathcal{R}_\nu^{+,0}$, $\mathcal{R}_\mu^{L,S}$

Turning to rare kaon decays, we define four SM-normalized ratios:

$$\mathcal{R}_\nu^+ = \frac{\mathcal{B}(K^+ \rightarrow \pi^+ \nu \bar{\nu})}{\mathcal{B}(K^+ \rightarrow \pi^+ \nu \bar{\nu})_{\text{SM}}}, \quad \mathcal{R}_\nu^0 = \frac{\mathcal{B}(K_L \rightarrow \pi^0 \nu \bar{\nu})}{\mathcal{B}(K_L \rightarrow \pi^0 \nu \bar{\nu})_{\text{SM}}}, \quad \mathcal{R}_\mu^{L(S)} = \frac{\mathcal{B}(K_{L(S)} \rightarrow \mu \mu)}{\mathcal{B}(K_{L(S)} \rightarrow \mu \mu)_{\text{SM}}}, \quad (4.2)$$

which all become unity in SM-limit. We note that the g2HDM contribution to all rare kaon decays (as well as $B_q \rightarrow \mu^+ \mu^-$, $B_d \rightarrow X_s \gamma$) considered originate from penguin diagrams involving H^+ and a top or charm quark.⁵ Therefore, the underlying flavor structure of NP contributions to these observables are similar if not highly correlated. We first give results for kaon decays as functions of κ and $(\varepsilon'/\varepsilon)_{\text{NP}}$. We subsequently highlight various correlations between these observables.

We give scan values of \mathcal{R}_ν^+ (upper) and \mathcal{R}_ν^0 (lower) vs κ , i.e. $\varepsilon_K^{\text{NP}}$, in Fig. 6. For light H^+ (left), we find $\mathcal{B}(K^+ \rightarrow \pi^+ \nu \bar{\nu})$ can be enhanced to 10–20% above SM. For $K_L \rightarrow \pi^0 \nu \bar{\nu}$, somewhat opposite effect is noticed: the \mathcal{R}_ν^0 remains either close to SM value or is slightly suppressed; the largest suppression reaching about 10%. For heavy H^+ case (right), the

⁵We tacitly drop the u -quark contribution from discussion. Flavor hierarchies suggest $|\rho_{tu}|$, $|\rho_{ut}|$ should be much less than charm counterparts, but we know rather little by direct measurement [99].

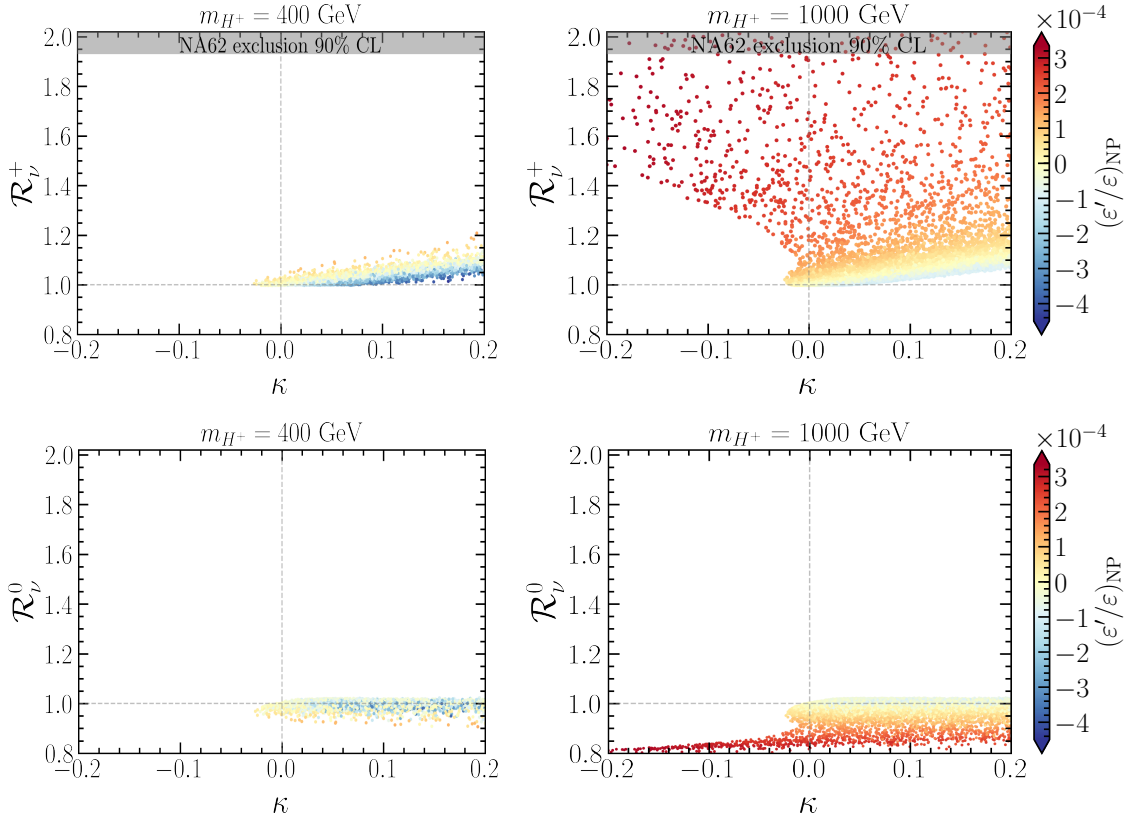


Figure 6. Ratios \mathcal{R}_{ν}^+ (upper) and \mathcal{R}_{ν}^0 (lower) as function of κ , and correlation with NP in ε'/ε .

results may appear a bit counterintuitive, as we see rather large effect for $K^+ \rightarrow \pi^+ \nu \bar{\nu}$, which can be enhanced to the upper limit of NA62 (actually reaching up to $\mathcal{R}_{\nu}^+ \lesssim 4$), while $K_L \rightarrow \pi^0 \nu \bar{\nu}$ can be suppressed by 20% compared to SM value.

We also illustrate in Fig. 6 the correlation of rare K decays with $(\varepsilon'/\varepsilon)_{\text{NP}}$. Large positive $(\varepsilon'/\varepsilon)_{\text{NP}}$ (red) correlates with larger effects in branching ratios, and negative values (blue) with smaller effects. Note also that for heavy H^+ , one can still have large effects in $\mathcal{R}_{\nu}^{+,0}$ despite $\kappa \sim 0$, especially for charged mode. *This highlights the importance of $K^+ \rightarrow \pi^+ \nu \bar{\nu}$ decay as a sensitive probe of heavy H^+ .*

4.3 $K \rightarrow \pi \nu \nu$ sensitivity to heavy charged Higgs

Before proceeding further, let us understand why the heavy H^+ case shows surprisingly large effects compared with light H^+ . The g2HDM contribution to $s \rightarrow d \nu \bar{\nu}$ is the second term of Eq. (3.28). Expanding the g2HDM part explicitly in terms of ρ_{ij} and CKM elements according to Eq. (3.27), focusing on the dominant top loop diagram we obtain (dropping

factor of $-\delta_{ab}/16\pi^2$)

$$\begin{aligned} \frac{C_{LL}^{a,b}}{v_t} &\Rightarrow \frac{\sum_j (V_{js}^* \rho_{jt}) \sum_k (\rho_{kt}^* V_{kd})}{V_{ts}^* V_{td}} G_Z(m_t^2/m_{H^+}^2) \\ &= \left(\rho_{tt} + \frac{V_{cs}^*}{V_{ts}^*} \rho_{ct} \right) \left(\rho_{tt}^* + \frac{V_{cd}}{V_{td}} \rho_{ct}^* \right) G_Z(m_t^2/m_{H^+}^2), \end{aligned} \quad (4.3)$$

where the two CKM factors associated with ρ_{ct} , $V_{cs}^*/V_{ts}^* \simeq -23.5 - 0.46i$, and $V_{cd}/V_{td} \simeq -22.8 - 9.4i$, respectively, are quite sizable. Thus, the $s \rightarrow d\nu\bar{\nu}$ process has rather special sensitivity to ρ_{ct} . Revisiting Fig. 4, we recall that the combined constraints from B sector plus ε_K restrict ρ_{ct} to very small values for light H^+ . But for heavy H^+ case, B sector constraints weaken considerably, then ε_K allows ρ_{ct} to become appreciable.

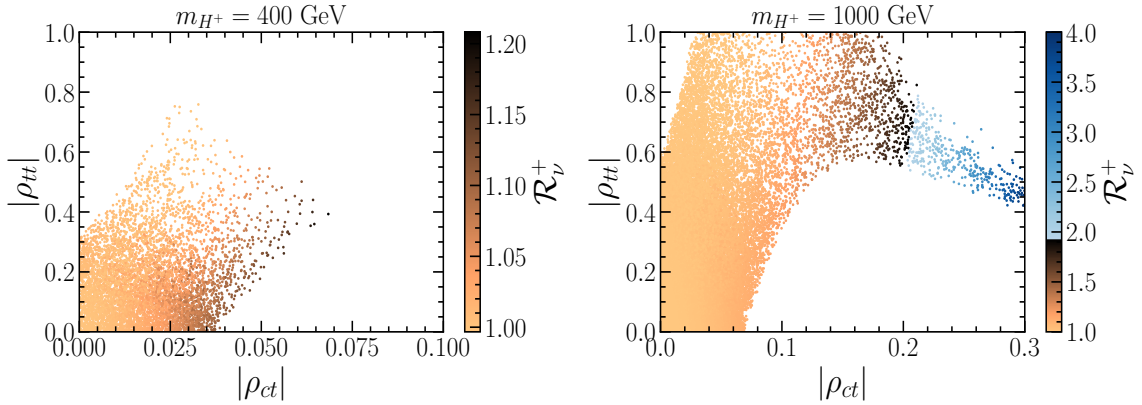


Figure 7. Scatter plot in $|\rho_{ct}|-|\rho_{tt}|$, correlated with \mathcal{R}_ν^+ after imposing flavor constraints.

We show in Fig. 7 the scatter in the $|\rho_{ct}|-|\rho_{tt}|$ plane, in correlation with \mathcal{R}_ν^+ . For light H^+ , $|\rho_{ct}|$ is highly constrained below ~ 0.06 , resulting in marginal enhancement of \mathcal{R}_ν^+ . But for heavy H^+ , much larger ρ_{ct} up to ~ 0.2 is allowed, and the aforementioned CKM factors then boost \mathcal{R}_ν^+ up to the NA62 limit. In fact, flavor constraints (B sector together with ε_K) do not rule out higher values (illustrated in blue) of \mathcal{R}_ν^+ , but cut off only by the NA62 bound itself. This further illustrates the significant role of $K^+ \rightarrow \pi^+ \nu\bar{\nu}$ in probing heavy H^+ , which was already alluded to in the previous subsection. Note also that enhancing \mathcal{R}_ν^+ requires a significant value for ρ_{tt} , but still less than unity. The dark points that saturate the NA62 bound in Fig. 7(right) are for $|\rho_{ct}|$ reaching ~ 0.2 , which one would not have anticipated based on the behavior seen in Fig. 7(left) for lighter m_{H^+} .

The contrasting behavior of the CP-violating counterpart $K_L \rightarrow \pi^0 \nu\bar{\nu}$ can be understood by noting that the purely ρ_{ct} term, which enjoys the largest CKM enhancement $|v_c/v_t| \simeq 580$, belongs to the CP-conserving part of NP, so $K_L \rightarrow \pi^0 \nu\bar{\nu}$ is not sensitive to this term. But $\rho_{tt}\rho_{ct}$ interference terms can have CP-violating phase. After expanding Eq. (4.3) in terms of ρ_{ij} and CKM elements, then putting back in Eq. (3.28), one obtains,

$$\begin{aligned} v_t X_{\text{eff}} &\simeq (-5.0 + 2.2i) - (96.4 + 0.06i)|\rho_{ct}|^2 - (0.15 - 0.06i)|\rho_{tt}|^2 \\ &\quad + (4.1 - 0.08i)\rho_{tt}\rho_{ct}^* + (3.6 - 1.5i)\rho_{tt}^*\rho_{ct}, \end{aligned} \quad (4.4)$$

where the first term is the SM contribution. We first note that the $|\rho_{ct}|^2$ and $|\rho_{tt}|^2$ terms are close to real, but $\rho_{tt}^*\rho_{ct}$ is complex. The imaginary part of $\rho_{tt}^*\rho_{ct}$ largely cancel between the two interference terms (and further suppressed by $|\rho_{ct}| < 0.2$). For the real part, the $-0.08i$ coefficient to $\rho_{tt}^*\rho_{ct}$ is small, but carries the same sign as the $-1.5i$ coefficient to $\rho_{tt}\rho_{ct}^*$, which explains the destructive interference with SM effect, as seen in Fig. 6.

Note that compared with ρ_{ct} , there is no similar sensitivity to ρ_{tc} . In fact, flavor constraints on ρ_{tc} are the poorest among the three top ρ_{ij} couplings considered. This is due to two reasons: first, ρ_{tc} is associated with the charm loop rather than top, hence the loop function is small; second, there is no CKM enhancement, i.e. $C_{LL}^{a,b}/v_t \propto |\rho_{tc}|^2$.

We have commented that the well-measured $K_L \rightarrow \mu^+\mu^-$ seems to prefer LD $A_{L\gamma\gamma}$ effect to be destructive against SD in Eq. (3.35). But $K_{L,S} \rightarrow \mu^+\mu^-$ interference can probe the sign of $A_{L\gamma\gamma}$ [53]. If constructive SD-LD interference turns out to be favored by data in the future, we see from Eq. (3.34) that the SM value is considerably higher than the experimental result of Eq. (3.35). But $K_L \rightarrow \mu^+\mu^-$ behaves similarly to $K^+ \rightarrow \pi^+\nu\bar{\nu}$, since one just replaces $Z\nu\nu$ by $Z\mu\mu$ in the diagrams, hence g2HDM effect always *enhance* the branching ratio (see Fig. 6) hence can never match Eq. (3.35). Thus, g2HDM in the parameter space we consider cannot offer a solution to the potential new emergent tension. For $K_S \rightarrow \mu^+\mu^-$, we find variation in \mathcal{R}_μ^S is never more than 2%, which we doubt LHCb can distinguish. Thus, neither $K_L \rightarrow \mu^+\mu^-$ nor $K_S \rightarrow \mu^+\mu^-$ are interesting in g2HDM.

CKM enhancement factors analogous to Eq. (4.3) was first touched upon in the discussion of $b \rightarrow s\gamma$ transitions [16], where only one CKM factor of ρ_{ct} gets $1/\lambda^2$ -enhanced ($\lambda = |V_{us}|$), the other being λ^2 -suppressed. Among the three ($b \rightarrow s, d$ and $s \rightarrow d$) type of penguins involving H^+ -top quark in the loop, the $s \rightarrow d$ penguin is unique in receiving double $1/\lambda^2$ -enhancement for both ρ_{ct} factors. Analogous subtle CKM enhancement effects have been discussed for the tree level [100] $B \rightarrow \ell\nu$ process, now between $\bar{u}b$ and $\bar{\ell}\nu$ bilinears. It was stressed that, if Belle II found the ratio $\mathcal{B}(B \rightarrow \mu\nu)/\mathcal{B}(B \rightarrow \tau\nu)$ would deviate from the SM value of 0.0045, it would not only rule out SM, but type II 2HDM as well [101], while proving $\rho_{tu} \neq 0$ in g2HDM. Another application of such CKM enhancement, rooted in the charged Higgs Yukawa interaction in Eq. 2.1, is the tree level $cg \rightarrow bH^+$ production process [10] mentioned in the Introduction, which is surprisingly efficient compared with intuition derived from type II 2HDM.

4.4 Correlations in $K \rightarrow \pi\nu\nu$ decays, and with $B_s \rightarrow \mu\mu$

We now discuss the correlations between rare K decays, and implications for g2HDM.

In Fig. 8, we show the correlation of $K^+ \rightarrow \pi^+\nu\bar{\nu}$ and $K_L \rightarrow \pi^0\nu\bar{\nu}$ by plotting \mathcal{R}_ν^+ vs \mathcal{R}_ν^0 as functions of κ (upper row) and $(\varepsilon'/\varepsilon)_{\text{NP}}$ (lower row). As already noted from Fig. 6, while opposite in behavior, the g2HDM effects are far more pronounced in $K^+ \rightarrow \pi^+\nu\bar{\nu}$ compared with $K_L \rightarrow \pi^0\nu\bar{\nu}$, for both $m_{H^+} = 400$ and 1000 GeV. Needless to say, the decays conform with the Grossman-Nir bound, $\mathcal{B}(K_L \rightarrow \pi^0\nu\bar{\nu}) \lesssim 4.3 \mathcal{B}(K^+ \rightarrow \pi^+\nu\bar{\nu})$ [102]. The future 10% measurement of $\mathcal{B}(K^+ \rightarrow \pi^+\nu\bar{\nu})$ by NA62, expected by 2024, could start to limit the amount of suppression possible for K_L decay. The fact that large negative values (blue points) of κ correlates with higher enhancement of $K^+ \rightarrow \pi^+\nu\bar{\nu}$ and suppression of $K_L \rightarrow \pi^0\nu\bar{\nu}$ was already obvious from Fig. 6, but it becomes visually more distinct in

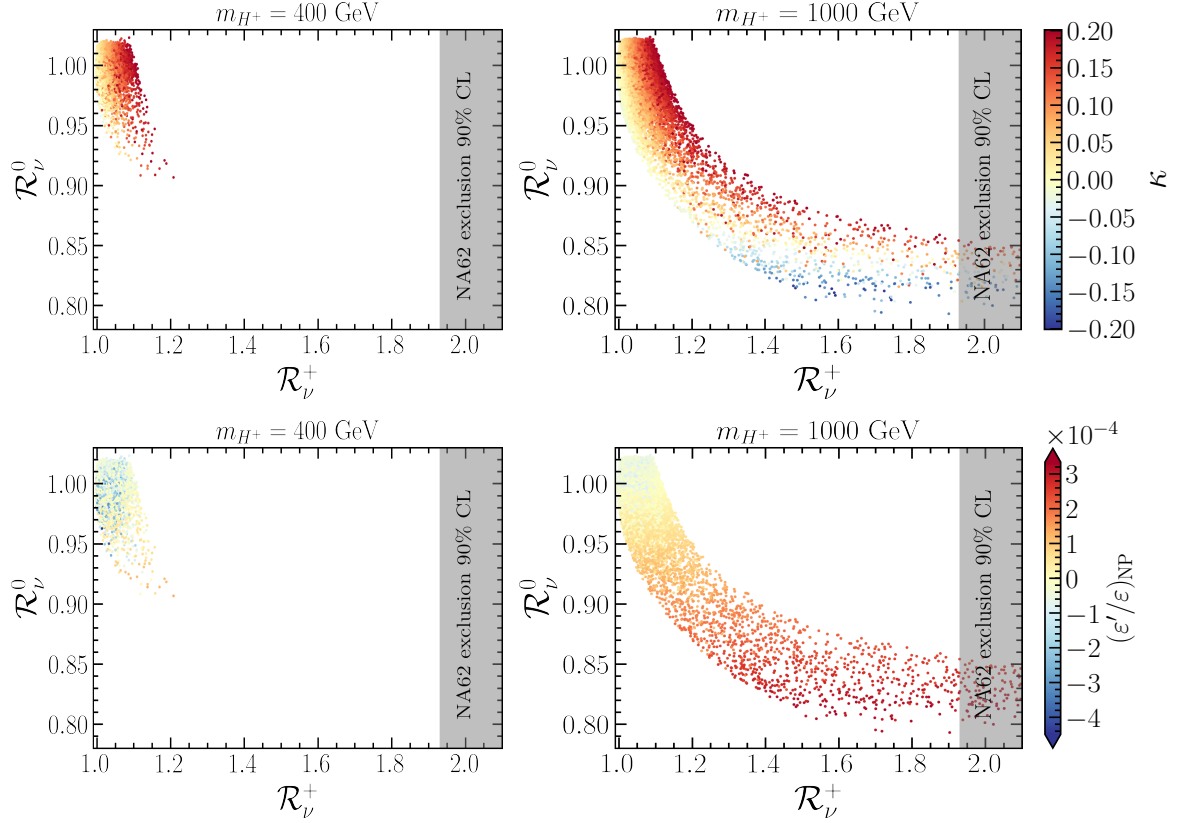


Figure 8. Correlations between $K^+ \rightarrow \pi^+ \nu \bar{\nu}$, $K_L \rightarrow \pi^0 \nu \bar{\nu}$, and κ (upper) and $(\epsilon'/\epsilon)_{\text{NP}}$ (lower).

Fig. 8 (upper row), where blue points lie on the lower end of the scatter plot. The opposite correlation is seen for $(\epsilon'/\epsilon)_{\text{NP}}$, where large positive values (red points) lie on the lower end of the scatter plot, while negative contributions (blue points) are closer to SM value. The upshot is that, with improved results from NA62 expected soon, we find $K^+ \rightarrow \pi^+ \nu \bar{\nu}$ would play the leading role in probing g2HDM in the coming future. The $K_L \rightarrow \pi^0 \nu \bar{\nu}$ mode can play the crucial role of confirming the unique g2HDM effects in the future, but the task would be challenging as it may require upgrades beyond KOTO Step-2 [88, 89] and KLEVER [87]. Similarly, measurement of ϵ'/ϵ at sensitivity of 10^{-4} is needed to probe g2HDM effects, which at present looks unlikely. Once again, this makes $K^+ \rightarrow \pi^+ \nu \bar{\nu}$ the leading kaon observable to watch out for.

Finally, it is of considerable interest to discuss the correlation between $K^+ \rightarrow \pi^+ \nu \bar{\nu}$ and $B_q \rightarrow \mu^+ \mu^-$. In Fig. 9, we plot $\mathcal{B}(B_s \rightarrow \mu^+ \mu^-)$ vs R_ν^+ , together with κ (upper row) and $(\epsilon'/\epsilon)_{\text{NP}}$ (lower row). For light H^+ , $\mathcal{B}(B_s \rightarrow \mu^+ \mu^-)$ mostly stays within 2σ range of the SM value of $(3.66 \pm 0.14) \times 10^{-9}$ [25], where dashed line indicates the central value, while R_ν^+ changes by less than $\sim 20\%$; large suppression of $B_s \rightarrow \mu\mu$ coupled with enhancement of $K^+ \rightarrow \pi^+ \nu \bar{\nu}$ is ruled out by current flavor data. But for heavy H^+ , the anti-correlation of g2HDM effects in $\mathcal{B}(B_s \rightarrow \mu^+ \mu^-)$ and R_ν^+ is clearly visible. This is of interest because the central value of LHCb [21, 22] at $\mathcal{B}(B_s \rightarrow \mu^+ \mu^-)$ at 3.09×10^{-9} is somewhat lower than

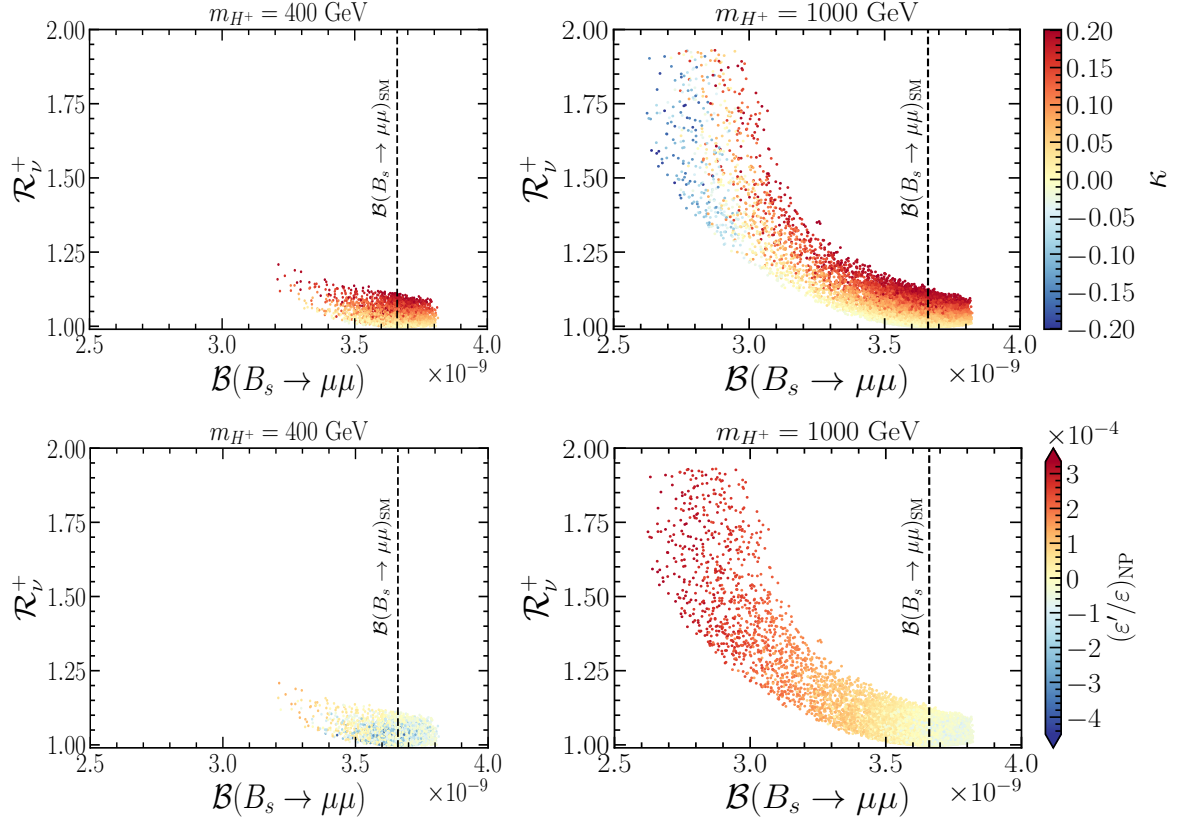


Figure 9. Correlations between $K^+ \rightarrow \pi^+ \nu \bar{\nu}$, $B_s \rightarrow \mu^+ \mu^-$, and κ (upper) and $(\epsilon'/\epsilon)_{\text{NP}}$ (lower).

SM, but the new full Run 2 result reported by CMS is fully consistent with SM.⁶ While the earlier impression that $B_s \rightarrow \mu\mu$ is slightly below SM seems to have gone away, some insight may be gained from kaon decay. The right plot of Fig. 9 shows that $\mathcal{B}(B_s \rightarrow \mu^+ \mu^-)$ can be suppressed in g2HDM for heavy H^+ . The correlation with higher values of \mathcal{R}_ν^+ then means the upcoming NA62 measurement could provide early tests of the size of g2HDM effects in $B_s \rightarrow \mu\mu$. This correlation is notable for both κ and $(\epsilon'/\epsilon)_{\text{NP}}$ in opposite way, more prominent for negative values of κ , but positive values for $(\epsilon'/\epsilon)_{\text{NP}}$.

Similar correlation is also observed for case of $B_d \rightarrow \mu\mu$, as can be seen from Fig. 10. The decay is not measured yet; the latest limit from LHCb [21, 22] based on Full Run 1 and Run 2 data reads $\mathcal{B}(B_d \rightarrow \mu\mu) < 2.6 \times 10^{-10}$ at 95% C.L, while the recent analysis from CMS collaboration giving a more precise limit $\mathcal{B}(B_d \rightarrow \mu\mu) < 1.9 \times 10^{-10}$ at 95% C.L. [23]. For the corresponding SM prediction, we find $\mathcal{B}(B_d \rightarrow \mu\mu)_{\text{SM}} = (1.14 \pm 0.12) \times 10^{-10}$, the central value of which is shown as black dashed line in Fig. 10.

⁶The even smaller central value of $\mathcal{B}(B_s \rightarrow \mu^+ \mu^-)_{\text{ave}} \simeq 2.69 \times 10^{-9}$ from combined [32] ATLAS, CMS and LHCb analysis based on data collected during 2011-2016 probably should no longer be considered.

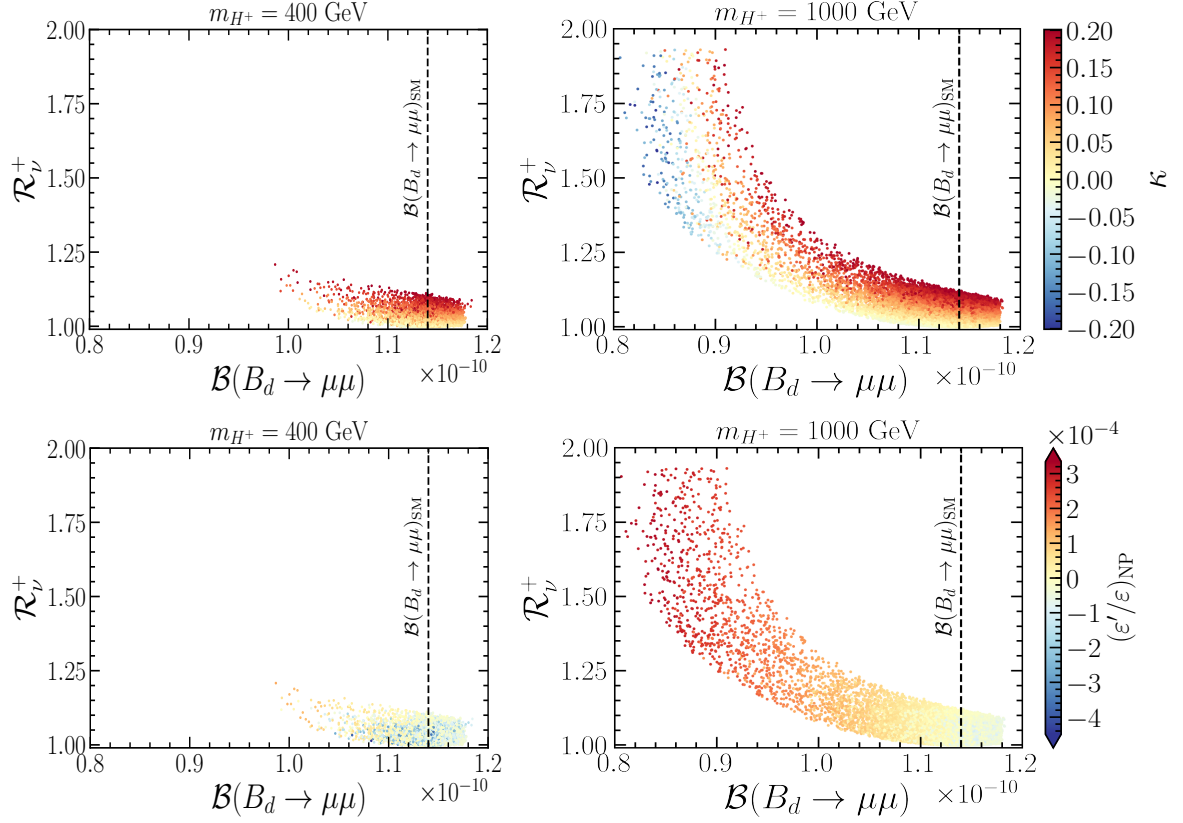


Figure 10. Correlations between $K^+ \rightarrow \pi^+ \nu \bar{\nu}$, $B_d \rightarrow \mu^+ \mu^-$, and κ (upper) and $(\varepsilon'/\varepsilon)_{\text{NP}}$ (lower).

5 Discussion and Summary

We return to discuss briefly the implications of the new CMS result [23] of $\mathcal{B}(B_s \rightarrow \mu\mu)$. Our results for light H^+ remains unaffected, as this scenario was already tightly constrained by B sector observables and ε_K . However, for heavy H^+ , there are important changes. After imposing 2σ range of CMS value in our parameter scan, the most significant consequences are for ε_K and $K^+ \rightarrow \pi^+ \nu \bar{\nu}$. For the former, we find $\kappa < 0$ gets mostly ruled out, and limited now to $[-0.05, 0.2]$. For the latter, we find \mathcal{R}_ν^+ can be enhanced only up to 50%, although we do find a few points reaching 80%. For $K_L \rightarrow \pi^0 \nu \bar{\nu}$, it can at best be suppressed by 15% compared to SM. No appreciable change for $(\varepsilon'/\varepsilon)_{\text{NP}}$ is observed, and all correlations discussed remain intact.

Before offering our summary, we comment on FCNH $t \rightarrow ch$ decay, where CMS recently set the most stringent limit [103] of $\mathcal{B}(t \rightarrow ch) < 0.094\%$ at 95% C.L., based on 137 fb^{-1} data at 13 TeV. This would put a constraint on the combination of $|c_\gamma \tilde{\rho}_{tc}|$, where $\tilde{\rho}_{tc} \equiv \sqrt{\rho_{tc}^2 + \rho_{ct}^2}/\sqrt{2}$. We find $|c_\gamma \tilde{\rho}_{tc}| < 0.059$, which can be evaded by having c_γ small enough. One may think the ACME bound on electron EDM, $|d_e|$, as the most challenging. But as alluded to in the Introduction, a hierarchy between g2HDM diagonal Yukawa couplings of top and electron $|\rho_{ee}/\rho_{tt}| \propto \lambda_e/\lambda_t$, which echoes the one seen already in SM Yukawa couplings helps one to handily evade [8] the ACME bound, by a couple orders of magnitude,

which should be watched.

In summary, we explore g2HDM contributions of extra top Yukawa couplings ρ_{ij} to several kaon processes, including kaon mixing, ε'/ε , and rare $K^+ \rightarrow \pi^+ \nu \bar{\nu}$, $K_L \rightarrow \pi^0 \nu \bar{\nu}$, and $K_{L,S} \rightarrow \mu\mu$ decays. We first point out that ε_K provides significant constraint on ρ_{ij} couplings that are complementary to the B sector, giving the leading constraint on the off-diagonal ρ_{ct} coupling. We consider two disparate masses of H^+ : 400 GeV and 1000 GeV. We find g2HDM contribution to $(\varepsilon'/\varepsilon)_{\text{NP}}$ as large as $\sim (1-3) \times 10^{-4}$ are achievable while satisfying B sector and ε_K constraints, with light H^+ preferring negative values reaching down to $\sim -5 \times 10^{-4}$. For rare $K \rightarrow \pi \nu \bar{\nu}$ decays, we find opposing effects in charged vs neutral modes. For light H^+ case, we find $K^+ \rightarrow \pi^+ \nu \bar{\nu}$ can be enhanced by up to $\sim 20\%$, while $K_L \rightarrow \pi^0 \nu \bar{\nu}$ can receive suppression up to $\sim 10\%$. However, for $m_{H^+} = 1000$ GeV, the B physics and ε_K constraints on ρ_{ij} become weaker, and sizable enhancements of kaon decays become possible. We find that $K^+ \rightarrow \pi^+ \nu \bar{\nu}$ can easily saturate the current NA62 bound, while $K_L \rightarrow \pi^0 \nu \bar{\nu}$ can be suppressed by up to 20% over the SM. For $K_L \rightarrow \mu\mu$, large theory errors make it ineffective as a probe for H^+ effects, while $K_S \rightarrow \mu^+ \mu^-$ remains SM-like in g2HDM. Exploring the correlation of $K^+ \rightarrow \pi^+ \nu \bar{\nu}$ with $B_s \rightarrow \mu^+ \mu^-$, we find for heavy $m_{H^+} = 1000$ GeV, enhanced $K^+ \rightarrow \pi^+ \nu \bar{\nu}$ in g2HDM implies suppression of $B_s \rightarrow \mu\mu$. Precise measurements of $\mathcal{B}(K^+ \rightarrow \pi^+ \nu \bar{\nu})$ and $\mathcal{B}(B_s \rightarrow \mu^+ \mu^-)$ should be able to distinguish the parameter space corresponding to sub-TeV vs TeV scale H^+ .

Acknowledgments This research is supported by MOST 110-2639-M-002-002-ASP of Taiwan, and NTU grants 110L104019 and 110L892101.

A Loop Functions

The loop functions related to $|\Delta F| = 2$ processes are [27],

$$F_1(a, b) = \frac{-1}{(1-a)(1-b)} + \frac{b^2 \log b}{(1-b)^2(a-b)} - \frac{a^2 \log a}{(1-a)^2(a-b)}, \quad (\text{A.1})$$

$$F_2(a, b, c) = \frac{-3a^2 \log a}{(a-1)(a-b)(a-c)} + \frac{b(4a-b) \log b}{(b-1)(a-b)(b-c)} + \frac{c(4a-c) \log c}{(c-1)(a-c)(c-b)}. \quad (\text{A.2})$$

The loop functions related to $|\Delta F| = 1$ processes $s \rightarrow df \bar{f}$ ($f = q, \ell, \nu$) are [26, 48],

$$G_{\gamma 1}(a) = -\frac{16 - 45a + 36a^2 - 7a^3 + 6(2 - 3a) \log a}{36(1-a)^4}, \quad (\text{A.3})$$

$$G_{\gamma 12}(a) = -\frac{2 - 9a + 18a^2 - 11a^3 + 6a^3 \log a}{36(1-a)^4} + \frac{2}{3}G_{\gamma 1}(a), \quad (\text{A.4})$$

$$G_Z(a) = \frac{a(1-a + \log a)}{2(1-a)^2}, \quad (\text{A.5})$$

and function related to $s \rightarrow dg$ is [26],

$$F_\sigma(a) = -\frac{2 + 3a - 6a^2 + a^3 + 6a \log a}{12(1-a)^4}. \quad (\text{A.6})$$

B Neutral B Meson Mixings and Mixing-induced CPV

The $\Delta B = 2$ effective Hamiltonian relevant for our purpose is given by,

$$\mathcal{H}_{\text{eff}}(\Delta B = 2) = (C_{HH}^{(q)} + C_{WH}^{(q)}) (\bar{b}\gamma^\mu P_L q)(\bar{b}\gamma^\mu P_L q) + \text{H.c.}, \quad (\text{B.1})$$

where $q = s, d$ corresponds to B_s - and B_d -mixing, respectively. The coefficients $C_{HH}^{(q)}$ and $C_{WH}^{(q)}$ are same as given in Eqs. (3.6) and (3.7) after obvious change of flavor indices.

The matrix element for \bar{B}_q - B_q mixing is defined as $M_{12}^{q*} = \langle \bar{B}_q | \mathcal{H}_{\text{eff}}(\Delta B = 2) | B_q \rangle$, where M_{12} is a complex quantity: $M_{12} \equiv |M_{12}| e^{2i\phi_q}$. Then absolute value of M_{12} determines the neutral B_q mass difference as,

$$\Delta M_{B_q} = 2|M_{12}^q| \equiv 2|M_{12}^q(\text{SM}) + M_{12}^q(\text{NP})|, \quad (\text{B.2})$$

while phases ϕ_q are convention dependent quantities and defined following Ref. [104] as,

$$\phi_s = \beta_s + \phi_s^{\text{NP}} \quad \phi_d = \beta_d + \phi_d^{\text{NP}}, \quad (\text{B.3})$$

with β_s and β given by CKM elements, $V_{ts} = -|V_{ts}|e^{-i\beta_s}$ and $V_{td} = |V_{td}|e^{-i\beta}$, and ϕ_q^{NP} is due to contribution from NP effective Hamiltonian in Eq. (B.1). The SM predictions [105] for mass differences are $\Delta M_{B_s} = (18.4_{-1.2}^{+0.7}) \text{ ps}^{-1}$ and $\Delta M_{B_d} = (0.533_{-0.036}^{+0.022}) \text{ ps}^{-1}$, and the corresponding experimental values are given in Table 1.

The mixing phases ϕ_q are inferred from the measurement of mixing-induced CP asymmetries $S_{\psi K_S}$ and $S_{\psi\phi}$ which appear as coefficients in the time-dependent asymmetries of $B_d \rightarrow \psi K_S$ and $B_s \rightarrow \psi\phi$,

$$A_{\text{CP}}^{\psi K_S} = S_{\psi K_S} \sin(\Delta M_d t), \quad A_{\text{CP}}^{\psi\phi} = S_{\psi\phi} \sin(\Delta M_s t). \quad (\text{B.4})$$

where in presence of NP phase ϕ_q^{NP} the CP asymmetries $S_{\psi K_S}$ and $S_{\psi\phi}$ are given by [104],

$$S_{\psi K_S} = \sin(2\beta + 2\phi_d^{\text{NP}}), \quad S_{\psi\phi} = \sin(2|\beta_s| - 2\phi_s^{\text{NP}}). \quad (\text{B.5})$$

References

- [1] T.D. Lee, Phys. Rev. D **8**, 1226 (1973).
- [2] G.C. Branco *et al.*, Phys. Rept. **516**, 1 (2012) [arXiv:1106.0034 [hep-ph]].
- [3] S.L. Glashow and S. Weinberg, Phys. Rev. D **15**, 1958 (1977)
- [4] W.-S. Hou, Phys. Lett. B **296**, 179 (1992).
- [5] S. Kanemura, Y. Okada and E. Senaha, Phys. Lett. B **606**, 361 (2005) [arXiv:hep-ph/0411354 [hep-ph]].
- [6] A.D. Sakharov, Pisma Zh. Eksp. Teor. Fiz. **5**, 32 (1967).
- [7] K. Fuyuto, W.-S. Hou and E. Senaha, Phys. Lett. B **776**, 402 (2018) [arXiv:1705.05034 [hep-ph]].
- [8] K. Fuyuto, W.-S. Hou and E. Senaha, Phys. Rev. D **101**, 011901 (2020) [arXiv:1910.12404 [hep-ph]].

- [9] M. Kohda, T. Modak and W.-S. Hou, Phys. Lett. B **776**, 379 (2018) [arXiv:1710.07260 [hep-ph]].
- [10] D.K. Ghosh, W.-S. Hou and T. Modak, Phys. Rev. Lett. **125**, 221801 (2020) [arXiv:1912.10613 [hep-ph]].
- [11] W.-S. Hou and T. Modak, Mod. Phys. Lett. A **36**, 2130006 (2021) [arXiv:2012.05735 [hep-ph]].
- [12] J. Baron *et al.* [ACME], Science **343**, 269 (2014) [arXiv:1310.7534 [physics.atom-ph]].
- [13] V. Andreev *et al.* [ACME], Nature **562**, 355 (2018).
- [14] S.M. Barr and A. Zee, Phys. Rev. Lett. **65**, 21 (1990) [erratum: Phys. Rev. Lett. **65**, 2920 (1990)].
- [15] Y.S. Amhis *et al.* [HFLAV], Eur. Phys. J. C **81**, 226 (2021) [arXiv:1909.12524 [hep-ex]].
- [16] B. Altunkaynak, W.-S. Hou, C. Kao, M. Kohda and B. McCoy, Phys. Lett. B **751**, 135 (2015) [arXiv:1506.00651 [hep-ph]].
- [17] A. Crivellin, A. Kokulu and C. Greub, Phys. Rev. D **87**, 094031 (2013) [arXiv:1303.5877 [hep-ph]].
- [18] M. Misiak *et al.*, Phys. Rev. Lett. **114**, 221801 (2015) [arXiv:1503.01789 [hep-ph]].
- [19] M. Misiak and M. Steinhauser, Eur. Phys. J. C **77**, 201 (2017) [arXiv:1702.04571 [hep-ph]].
- [20] W.-S. Hou, G. Kumar, T. Modak, in prepration.
- [21] R. Aaij *et al.* [LHCb], Phys. Rev. Lett. **128**, 041801 (2022) [arXiv:2108.09284 [hep-ex]].
- [22] R. Aaij *et al.* [LHCb], Phys. Rev. D **105**, 012010 (2022) [arXiv:2108.09283 [hep-ex]].
- [23] CMS Collaboration, CMS-PAS-BPH-21-006, <https://cds.cern.ch/record/2815334>.
- [24] C. Bobeth, M. Gorbahn, T. Hermann, M. Misiak, E. Stamou and M. Steinhauser, Phys. Rev. Lett. **112** (2014), 101801 [arXiv:1311.0903 [hep-ph]].
- [25] M. Beneke, C. Bobeth and R. Szafron, JHEP **10**, 232 (2019) [arXiv:1908.07011 [hep-ph]].
- [26] S. Iguro and K. Tobe, Nucl. Phys. B **925**, 560 (2017) [arXiv:1708.06176 [hep-ph]].
- [27] A. Crivellin, D. Müller and C. Wiegand, JHEP **06**, 119 (2019) [arXiv:1903.10440 [hep-ph]].
- [28] W.-S. Hou and G. Kumar, Phys. Rev. D **102**, 115017 (2020) [arXiv:2008.08469 [hep-ph]].
- [29] M. Aaboud *et al.* [ATLAS], JHEP **04**, 098 (2019) [arXiv:1812.03017 [hep-ex]].
- [30] A.M. Sirunyan *et al.* [CMS], JHEP **04**, 188 (2020) [arXiv:1910.12127 [hep-ex]].
- [31] R. Aaij *et al.* [LHCb], Phys. Rev. Lett. **118**, 191801 (2017) [arXiv:1703.05747 [hep-ex]].
- [32] LHCb, ATLAS and CMS, LHCb-CONF-2020-002.
- [33] D. London and J. Matias, arXiv:2110.13270 [hep-ph].
- [34] G.W.-S. Hou, Int. J. Mod. Phys. A **34**, 1930002 (2019) [arXiv:1901.04033 [hep-ex]].
- [35] S. Iguro and Y. Omura, JHEP **05** (2018), 173 [arXiv:1802.01732 [hep-ph]].
- [36] P. Athron, C. Balazs, T.E. Gonzalo, D. Jacob, F. Mahmoudi and C. Sierra, JHEP **01** (2022), 037 [arXiv:2111.10464 [hep-ph]].
- [37] S. Iguro, Phys. Rev. D **105**, 095011 (2022) [arXiv:2201.06565 [hep-ph]].

- [38] M. Blanke, S. Iguro and H. Zhang, JHEP **06**, 043 (2022) [arXiv:2202.10468 [hep-ph]].
- [39] A.J. Buras, arXiv:hep-ph/9806471 [hep-ph].
- [40] V. Cirigliano, G. Ecker, H. Neufeld, A. Pich and J. Portoles, Rev. Mod. Phys. **84** (2012), 399 [arXiv:1107.6001 [hep-ph]].
- [41] A.J. Buras, J.-M. Gérard and W.A. Bardeen, Eur. Phys. J. C **74**, 2871 (2014) [arXiv:1401.1385 [hep-ph]].
- [42] Z. Bai *et al.* [RBC and UKQCD], Phys. Rev. Lett. **115**, 212001 (2015) [arXiv:1505.07863 [hep-lat]].
- [43] J.R. Batley *et al.* [NA48], Phys. Lett. B **544**, 97 (2002) [arXiv:hep-ex/0208009 [hep-ex]].
- [44] A. Alavi-Harati *et al.* [KTeV], Phys. Rev. D **67**, 012005 (2003) [erratum: Phys. Rev. D **70**, 079904 (2004)] [arXiv:hep-ex/0208007 [hep-ex]].
- [45] E. Abouzaid *et al.* [KTeV], Phys. Rev. D **83**, 092001 (2011) [arXiv:1011.0127 [hep-ex]].
- [46] C.-H. Chen and T. Nomura, JHEP **08**, 145 (2018) [arXiv:1804.06017 [hep-ph]].
- [47] C.-H. Chen and T. Nomura, Phys. Lett. B **787**, 182 (2018) [arXiv:1805.07522 [hep-ph]].
- [48] S. Iguro and Y. Omura, JHEP **08**, 098 (2019) [arXiv:1905.11778 [hep-ph]].
- [49] R. Abbott *et al.* [RBC and UKQCD], Phys. Rev. D **102**, 054509 (2020) [arXiv:2004.09440 [hep-lat]].
- [50] J. Aebischer, C. Bobeth and A.J. Buras, Eur. Phys. J. C **80**, 705 (2020) [arXiv:2005.05978 [hep-ph]].
- [51] G. Ecker and A. Pich, Nucl. Phys. B **366**, 189 (1991)
- [52] G. Isidori and R. Unterdorfer, JHEP **01**, 009 (2004) [arXiv:hep-ph/0311084 [hep-ph]].
- [53] G. D’Ambrosio and T. Kitahara, Phys. Rev. Lett. **119**, 201802 (2017) [arXiv:1707.06999 [hep-ph]].
- [54] F. Mescia, C. Smith and S. Trine, JHEP **08**, 088 (2006) [arXiv:hep-ph/0606081 [hep-ph]].
- [55] A. Dery, M. Ghosh, Y. Grossman and S. Schacht, JHEP **07** (2021), 103 [arXiv:2104.06427 [hep-ph]].
- [56] S. Davidson and H.E. Haber, Phys. Rev. D **72**, 035004 (2005) [erratum: Phys. Rev. D **72**, 099902 (2005)] [arXiv:hep-ph/0504050].
- [57] W.-S. Hou and M. Kikuchi, EPL **123**, 11001 (2018) [arXiv:1706.07694 [hep-ph]].
- [58] P.A. Zyla *et al.* [Particle Data Group], PTEP **2020**, 083C01 (2020).
- [59] A.J. Buras and D. Guadagnoli, Phys. Rev. D **78**, 033005 (2008) [arXiv:0805.3887 [hep-ph]].
- [60] M. Bona *et al.* [UTfit], JHEP **10** (2006), 081 [arXiv:hep-ph/0606167 [hep-ph]], updates available on <http://www.utfit.org/UTfit/>.
- [61] J. Charles *et al.*, Phys. Rev. D **91**, 073007 (2015) [arXiv:1501.05013 [hep-ph]]; updates available on <https://ckmfitter.in2p3.fr/>.
- [62] J. Brod, M. Gorbahn and E. Stamou, Phys. Rev. Lett. **125**, 171803 (2020) [arXiv:1911.06822 [hep-ph]].
- [63] J. Aebischer, A. J. Buras and J. Kumar, JHEP **12**, 097 (2020) [arXiv:2006.01138 [hep-ph]].

- [64] V. Cirigliano, G. Ecker, H. Neufeld and A. Pich, *Eur. Phys. J. C* **33**, 369 (2004) [arXiv:hep-ph/0310351 [hep-ph]].
- [65] A.J. Buras, M. Gorbahn, S. Jäger and M. Jamin, *JHEP* **11**, 202 (2015) [arXiv:1507.06345 [hep-ph]].
- [66] V. Cirigliano, H. Gisbert, A. Pich and A. Rodríguez-Sánchez, *JHEP* **02**, 032 (2020) [arXiv:1911.01359 [hep-ph]].
- [67] T. Blum *et al.*, *Phys. Rev. D* **91**, 074502 (2015) [arXiv:1502.00263 [hep-lat]].
- [68] J. Aebischer, A.J. Buras and J.-M. Gérard, *JHEP* **02**, 021 (2019) [arXiv:1807.01709 [hep-ph]].
- [69] M. Gorbahn and U. Haisch, *Phys. Rev. Lett.* **97**, 122002 (2006) [arXiv:hep-ph/0605203 [hep-ph]].
- [70] V. Chobanova, G. D’Ambrosio, T. Kitahara, M. Lucio Martinez, D. Martinez Santos, I.S. Fernandez and K. Yamamoto, *JHEP* **05**, 024 (2018) [arXiv:1711.11030 [hep-ph]].
- [71] Y. Aoki *et al.*, arXiv:2111.09849 [hep-lat].
- [72] A.J. Buras, D. Buttazzo, J. Girrbach-Noe and R. Knegjens, *JHEP* **11**, 033 (2015) [arXiv:1503.02693 [hep-ph]].
- [73] F. Mescia and C. Smith, *Phys. Rev. D* **76**, 034017 (2007) [arXiv:0705.2025 [hep-ph]].
- [74] J. Brod, M. Gorbahn and E. Stamou, *PoS BEAUTY2020*, 056 (2021) [arXiv:2105.02868 [hep-ph]].
- [75] A.J. Buras, M. Gorbahn, U. Haisch and U. Nierste, *Phys. Rev. Lett.* **95**, 261805 (2005) [arXiv:hep-ph/0508165 [hep-ph]].
- [76] A.J. Buras, M. Gorbahn, U. Haisch and U. Nierste, *JHEP* **11**, 002 (2006) [erratum: *JHEP* **11**, 167 (2012)] [arXiv:hep-ph/0603079 [hep-ph]].
- [77] J. Brod and M. Gorbahn, *Phys. Rev. D* **78**, 034006 (2008) [arXiv:0805.4119 [hep-ph]].
- [78] G. Isidori, F. Mescia and C. Smith, *Nucl. Phys. B* **718**, 319 (2005) [arXiv:hep-ph/0503107 [hep-ph]].
- [79] A.J. Buras and E. Venturini, arXiv:2109.11032 [hep-ph].
- [80] E. Cortina Gil *et al.* [NA62], *JHEP* **06**, 093 (2021) [arXiv:2103.15389 [hep-ex]].
- [81] A.V. Artamonov *et al.* [BNL-E949], *Phys. Rev. D* **79**, 092004 (2009) [arXiv:0903.0030 [hep-ex]].
- [82] NA62 and KLEVER collaborations, arXiv:2009.10941 [hep-ex].
- [83] C.Q. Geng and J.N. Ng, *Phys. Rev. D* **38**, 2857 (1988) [erratum: *Phys. Rev. D* **41**, 1715 (1990)].
- [84] J.K. Ahn *et al.* [KOTO], *Phys. Rev. Lett.* **126**, 121801 (2021) [arXiv:2012.07571 [hep-ex]].
- [85] J.K. Ahn *et al.* [KOTO], *Phys. Rev. Lett.* **122**, 021802 (2019) [arXiv:1810.09655 [hep-ex]].
- [86] K. Shiomi [KOTO], *PoS BEAUTY2020*, 055 (2021)
- [87] F. Ambrosino *et al.* [KLEVER], arXiv:1901.03099 [hep-ex].
- [88] T. Nomura, *J. Phys. Conf. Ser.* **1526**, 012027 (2020).
- [89] K. Aoki *et al.*, arXiv:2110.04462 [nucl-ex].
- [90] D. Ambrose *et al.* [E871], *Phys. Rev. Lett.* **84**, 1389 (2000).

- [91] T. Akagi *et al.*, Phys. Rev. D **51**, 2061 (1995).
- [92] A. Heinson *et al.* [E791], Phys. Rev. D **51**, 985 (1995).
- [93] R. Aaij *et al.* [LHCb], Phys. Rev. Lett. **125**, 231801 (2020) [arXiv:2001.10354 [hep-ex]].
- [94] R. Aaij *et al.* [LHCb], Eur. Phys. J. C **77**, 678 (2017) [arXiv:1706.00758 [hep-ex]].
- [95] A. Cerri *et al.*, CERN Yellow Rep. Monogr. **7**, 867 (2019) [arXiv:1812.07638 [hep-ph]].
- [96] D.M. Straub, arXiv:1810.08132 [hep-ph].
- [97] J. Aebischer *et al.*, Comput. Phys. Commun. **232**, 71 (2018) [arXiv:1712.05298 [hep-ph]].
- [98] J. Aebischer, J. Kumar and D.M. Straub, Eur. Phys. J. C **78**, 1026 (2018) [arXiv:1804.05033 [hep-ph]].
- [99] For some discussion, see e.g. W.-S. Hou, T.-H. Hsu and T. Modak, Phys. Rev. D **102**, 055006 (2020) [arXiv:2008.02573 [hep-ph]].
- [100] W.-S. Hou, M. Kohda, T. Modak and G.-G. Wong, Phys. Lett. B **800**, 135105 (2020) [arXiv:1903.03016 [hep-ph]].
- [101] P. Chang, K.-F. Chen and W.-S. Hou, Prog. Part. Nucl. Phys. **97**, 261 (2017) [arXiv:1708.03793 [hep-ph]].
- [102] Y. Grossman and Y. Nir, Phys. Lett. B **398**, 163 (1997) [arXiv:hep-ph/9701313 [hep-ph]].
- [103] A. Tumasyan *et al.* [CMS], JHEP **02**, 169 (2022) [arXiv:2112.09734 [hep-ex]].
- [104] A.J. Buras and J. Girrbach, Rept. Prog. Phys. **77**, 086201 (2014) [arXiv:1306.3775 [hep-ph]].
- [105] L. Di Luzio, M. Kirk, A. Lenz and T. Rauh, JHEP **12**, 009 (2019) [arXiv:1909.11087 [hep-ph]].